

Pseudospectral calculation of the wave function of helium and the negative hydrogen ion

Paul E. Grabowski*

Department of Physics, Cornell University, Ithaca, New York 14853, USA

David F. Chernoff†

Department of Astronomy, Cornell University, Ithaca, New York 14853, USA

(Received 8 October 2009; published 8 March 2010)

We study the numerical solution of the nonrelativistic Schrödinger equation for two-electron atoms in ground and excited S states using pseudospectral (PS) methods of calculation. The calculation achieves convergence rates for the energy, Cauchy error in the wave function, and variance in local energy that are exponentially fast for all practical purposes. The method requires three separate subdomains to handle the wave function's cusplike behavior near the two-particle coalescences. The use of three subdomains is essential to maintaining exponential convergence and is more computationally efficient than a single subdomain. A comparison of several different treatments of the cusps suggests that the simplest prescription is sufficient. We investigate two alternate methods for handling the semi-infinite domain, one which involves a sequence of truncated versions of the domain and the other which employs an algebraic mapping of the semi-infinite domain to a finite one and imposes no explicit cutoffs on the wave function. The latter prescription proves superior. For many purposes it proves unnecessary to handle the three-particle coalescence in a special way. The presence of logarithmic terms in the exact solution is expected to limit the convergence to being nonexponential but the only clear evidence of that is the rate of convergence of derivatives near the three-particle coalescence point. Higher resolution than achieved in this work will ultimately be needed to see its limiting effect on other measures of error. As developed and applied here the PS method has many virtues: no explicit assumptions need be made about the asymptotic behavior of the wave function near cusps or at large distances, the local energy ($\mathcal{H}\psi/\psi$) is exactly equal to the calculated global energy at all collocation points, local errors go down everywhere with increasing resolution, the effective basis using Chebyshev polynomials is complete and simple, and the method is easily extensible to other bound states. As the number of collocation points grows, the method achieves exponential convergence up to the resolution tested. This study serves as a proof-of-principle of the method for more general two- and possibly three-electron applications.

DOI: [10.1103/PhysRevA.81.032508](https://doi.org/10.1103/PhysRevA.81.032508)

PACS number(s): 31.15.ac, 03.65.Ge, 02.70.Jn, 02.60.Lj

I. INTRODUCTION

The nonrelativistic, two-electron atom (H^- , He, Li^+) is the simplest “hard” problem in quantum mechanics. It involves strong electron-electron correlations, nontrivial symmetry considerations, and single as well as double continua. Many different solution techniques have been developed and applied over the past 80 years. A thorough understanding of this simple system is important not only because of its direct relevance to experimental studies in atomic physics but also because the best methods of solution may suggest generalizations applicable to multielectron and/or multiatom systems.

Our own interest in this problem arose from investigating bound-free and free-free opacity of the negative hydrogen ion H^- . As first conjectured by Wildt [1], H^- gives the greatest contribution to opacity in the atmosphere of the Sun and many other stars. The photo-absorption cross section of H^- is known to an accuracy of a few percentage points [2] but little attention has been devoted to H^- in less-than-ideal circumstances (high density, high magnetic field, etc.) of relevance to astrophysical applications. We sought a first-principles approach that would allow “exact” calculations of initial and final states as part

of these investigations and were led to reconsider this classic problem.

Ideally, there would exist a simple method capable of handling any two-electron state in the presence of a nucleus with any angular momentum whether bound or free. In practice, many individual methods have been formulated each having somewhat more specific goals. A common starting point, for example, is finding the ground-state energy for zero total angular momentum.

It is not possible in a single article, let alone an introduction, to review the full range of methods that have been developed and explored. We can briefly compare the strengths and weaknesses of a few select approaches by assessing each in terms of the generality (is it applicable to all states or just the ground state?), the capability of achieving an exact solution of the nonrelativistic Schrödinger equation in the limit of infinite nuclear mass (is it *in principle* capable of finding an exact solution [in the aforementioned sense] or are there intrinsic approximations?), the degree of tuning required (is it straightforward to apply or does it require an enlightened guess for, say, the choice of basis functions?), and, of course, the computational effort for a given level of accuracy.

The asymptotic rate of convergence of some error R_n as a function of the number n of basis functions, grid size, etc., is of central importance in evaluating a numerical method. To characterize the convergence rate the definitions of Boyd [3]

*peg9@cornell.edu

†chernoff@astro.cornell.edu

are used in this article and reproduced here. The algebraic index of convergence, k is defined as the maximum k so that

$$\lim_{n \rightarrow \infty} |R_n| n^k < \infty. \quad (1)$$

If k is finite then R_n converges algebraically. The simplest example of algebraic convergence is an error $R_n \propto 1/n^k$. If k is infinite then R_n converges exponentially. This latter category is subdivided into three cases defined by the value of

$$l = \lim_{n \rightarrow \infty} \frac{\log |R_n|}{n}. \quad (2)$$

If l is zero, a finite positive number, or infinite, the rate is subgeometric, geometric, or supergeometric, respectively. For example, if the error $R_n \propto \exp(-n^m)$, the conditions $0 < m < 1$, $m = 1$, and $m > 1$ correspond to subgeometric, geometric, and supergeometric convergence, respectively.

A. Variational method for two electrons and nucleus: ground state

The first numerical explorations of two-electron ground states adopted the approach of minimizing the global energy. Once Hylleraas determined that only three coordinates were needed to represent the wave function for S states he carried out such variational calculations (prior to the advent of computers) [4]. Pekeris and coworkers [5–8] did the first high precision calculations on computers, expanding the wave function in terms of Laguerre polynomials of linear combinations of the interparticle distances times an appropriate exponential falloff. They determined the energy of H^- to eight decimal places and that of He to nine, calculations that were the gold standard for several decades.

Variational methods have been highly successful at calculating extremely precise eigenvalues of the ground state of two-electron atoms. Indeed, eigenvalue energies have been calculated to numerical accuracy—at least 42 digits—that *far* exceeds the accuracy of the underlying physical description based on nonrelativistic equations of motion [9–19]. A clear strength of the general variational approach is that intrinsic approximations to the Hamiltonian operator need not be made. The principle drawbacks are related to the difficulties inherent in the selection of the basis: it should be complete so that convergence to the exact solution is possible and efficient so that finite numbers of elements do a good job representing the wave function.

Significant progress in choice of the basis for the two-electron problem has taken place. The inclusion of new functions (e.g., logarithmic terms) typically motivated by known limiting forms of the wave function improves the rate of convergence [7,9,11,20–24]. Furthermore, without special additions, some bases are simply incapable of representing the exact solution [25,26]. Klahn and Morgan have shown that there are examples where the expectation value of an operator (i.e., r^k with $k \geq 6$) converges to the incorrect value or diverges even if the basis is complete. In their example the basis cannot accurately represent the derivatives of the hydrogenic solution at $r = 0$ [27]. When employing such bases, one must always check that the physical property one is calculating is converging properly.

Schwartz [28] surveyed the convergence rate of the error in the ground-state energy eigenvalue achieved by many different strategies for basis set selection. His results for the error may be expressed as a function of n , the total number of basis functions selected according to a well-defined procedure. The error generally converges algebraically with index, $1.5 \leq k \leq 8.3$ ($\propto n^{-k}$), depending on the basis. The range in k highlights the significance that a good choice of basis can have on the asymptotic convergence of a calculation. One basis set, which included a single power of a logarithm, appeared to converge exponentially fast as σ^{-n} with σ in the range 0.51–0.54. Such exponential behavior is often assumed of variational methods if the basis can accurately describe the behavior of the wave function everywhere. That is, the basis includes functions which have the same analytic and nonanalytic behavior as the exact solution.

Loosely speaking, even when convergence is assured, the accuracy of the variationally inferred wave function (by many different measures) is much less than that of the energy eigenvalue. Parts of the wave function that have a small effect on the total energy are not well-constrained by lowering the energy. An alternative strategy to minimizing the global energy is to minimize the variance in the local energy instead [29–31]. This approach can produce better local values of the wave function but leads to nonlinear minimization problems which are more difficult to handle numerically (minimization of the variance in local energy with respect to parameters in the trial wave function) but still tractable because one need not calculate the global energy at each step.

B. Variational method for excited states

Variational methods [6,8,10,32,33] have been successful at calculating precise excitation energies. In general, variational methods extend naturally to excited, bound states whenever the variational parameters enter in a linear fashion. It is then straightforward to find multiple eigenstates of the linear system. The more highly excited the state the less converged the energy is, especially if the basis was optimized in order to reproduce the features of the ground state only.¹

C. Fourier spectral expansion

Griebel and Hamaekers [34] developed a Fourier expansion method for multidimensional quantum mechanical systems. They apply the hyperbolic cross truncation to their basis and show that for smooth solutions the exponential convergence

¹Drake [10] points out that alternative methods can calculate the singly excited spectrum. For high angular momentum, the system can be treated as an electron in the field of a perturbed core with higher and higher moments of the core being included for higher and higher accuracy. This calculation can be done analytically for the two-electron problem. The approximation here is that the electron correlation energy is ignored, but this is very small for such states. For large principle quantum numbers, quantum defect approximations work well. The energy is proportional to $1/(n - \delta_l)^2$, instead of the usual $1/n^2$, where n is the principle quantum number of the excited electron, l is its angular momentum, and δ_l gives the effect of the screening due to the inner electron.

rate is not dependent on the dimensionality of the system. They calculate the energies of several different systems including hydrogen and helium. Unfortunately, they fail to achieve exponential convergence because the cusps were not properly treated, and hence their highest resolution runs for hydrogen and helium are only good to about 2 and 10%, respectively.

D. Specialized methods for two-electron systems

Haftel and Mandelzweig and later other collaborators [35–41] have presented an exact treatment of two-electron atoms that begins by factoring out the correct cusp behavior and posing the problem in terms of the remaining part of the wave function. This piece which is continuous up to first derivatives is expanded in terms of hyperspherical harmonics yielding a set of coupled ordinary differential equations for coefficients which are functions of the hyperradius. The method fully accounts for the asymptotic behavior near coalescence points and yields results with energies good to one part in 10^9 . The hyperspherical harmonic expansion converges more quickly than if the cusp is not explicitly accommodated for but remains algebraic because of the higher-order discontinuities. The method accurately determines bound excited states as well.

E. Direct solution of partial differential equation for bound and continuum states

Most of the bound-state techniques mentioned thus far are unsuitable for calculating continuum states. In fact, continuum-state calculations rely on totally different variational methods. The main ones are R -matrix [42], Schwinger variational [43], and the complex Kohn variational [44] methods. Accuracy for these methods lags far behind that of bound-state calculations.

Roughly speaking, the source of some of these difficulties is related to describing the wave function over an infinite volume while simultaneously controlling the errors of greatest significance. Typically, linear variational methods are equivalent to spectral expansions of the wave function. The control one has over the accuracy of an approximate description of the wave function is indirect via the choice of the expansion. Instead, one may be motivated for both bound and continuum problems to consider solving the partial differential equation directly on a grid where a greater degree of local control is possible.

Finite difference methods (FDM) [45–48] and finite element methods (FEM) [49–54] represent the solution and the differential equation on a discrete grid. The FDM grid is usually evenly spaced with derivatives calculated to some small (usually second) order. FEM uses subdomains, concentrating grid points where more accuracy is needed. Recent work achieves as many as seven decimal places in the energy of the ground state but produces surprisingly nonsmooth wave functions [53,54]. The rate of convergence of these methods is limited by the order of the representation of derivatives and is always algebraic with some small index dependent on the order used for derivatives.

F. Pseudospectral approach

Some of the above considerations motivate an investigation of the pseudospectral (PS) method. Like FDM and FEM methods the PS method represents the wave function by values on a

discrete grid of points rather than by coefficients of a spectral expansion. However, the points are selected in a different manner and the derivative order increases with grid resolution. Roots of Jacobi polynomials are chosen in order to make the asymptotic rate of convergence of an analytic function constant across the entire finite nonperiodic domain. Such a choice also has the advantage that exponential convergence can be lost only by nonanalytic behavior within the domain. By contrast, an equispaced grid is sensitive to singularities nearby in the complex plane and can lead to divergences when interpolating near the endpoints (Runge phenomenon). Of all the Jacobi polynomials, Chebyshev polynomials vary the least over $[-1, 1]$ and hence produce the smallest residual from the PS method. The mathematical theory of nonsmooth functions is not well developed and precise convergence rates are usually calculated empirically [55].

The PS method [3,55,56] has seen successes in many fields including fluid dynamics [57], relativistic astrophysics [58], and numerical relativity [59,60]. When the underlying solution is smooth, the PS method typically requires less computational run time and less memory than FDM and FEM to achieve comparable precision. The method has been applied in quantum mechanics to solve the full Schrödinger equation for a single electron [61–63]. In addition, various simplifications of the multielectron Schrödinger equation have been treated, including the Hartree-Fock approximation [64–69], Møller-Plesset perturbation theory [70], and density functional theory [71,72].

To the authors' knowledge, no one has solved the full three-dimensional Schrödinger equation for heliumlike systems (the "exact" problem) using PS methods. This article implements the method, investigates several design choices and calculates ground and excited bound S states. The convergence rate is used as the metric to characterize different grid choices, alternative methods for handling regularity conditions and other practical considerations needed for an efficient algorithm. No attempt to reproduce the ultrahigh precision results of variational methods is made. The calculation employs a standard Chebyshev basis without any specialized tuning. The eigenvalue and eigenfunction problems are solved by a standard method. All calculations are done on a single processor with a speed of 6 GHz and 8 GB of memory.

The PS method is expected to be supergeometric on a finite computational domain if no singularities exist in the solution anywhere in the complex plane, geometric if singularities are only outside the domain, and algebraic if singularities exist within domain. If the domain is infinite or semi-infinite, subgeometric convergence is expected when no singularities are in the domain, and algebraic convergence is expected otherwise [3].

II. SETTING UP THE PROBLEM

Let \mathbf{z}_i and ∇_i^2 be the position vector and the Laplacian of the coordinates, respectively, of the i th electron if i is 1 or 2 and of the nucleus if i is 3. The nonrelativistic Schrödinger equation for a heliumlike system is

$$\mathcal{H} = -\frac{1}{2} \left(\frac{\nabla_1^2}{m} + \frac{\nabla_2^2}{m} + \frac{\nabla_3^2}{M} \right) + \mathcal{V}, \quad (3)$$

where

$$\mathcal{V} = -\frac{Z}{|\mathbf{z}_1 - \mathbf{z}_3|} - \frac{Z}{|\mathbf{z}_2 - \mathbf{z}_3|} + \frac{\alpha}{|\mathbf{z}_1 - \mathbf{z}_2|}, \quad (4)$$

Z is the nuclear charge, $\alpha = 1$ unless the electron-electron interaction is suppressed ($\alpha = 0$), m is the mass of the electron, and M is the mass of the nucleus. The units are $e = \hbar = 1/4\pi\epsilon_0 = 1$. The Hamiltonian acts on functions of nine dimensions, i.e., three coordinate positions for each particle.

The relative and center of mass coordinates are

$$\mathbf{r}_1 = \mathbf{z}_1 - \mathbf{z}_3 \quad (5)$$

$$\mathbf{r}_2 = \mathbf{z}_2 - \mathbf{z}_3 \quad (6)$$

$$\mathbf{R} = \frac{m(\mathbf{z}_1 + \mathbf{z}_2) + M\mathbf{z}_3}{M + 2m}. \quad (7)$$

Define the coordinates

$$r_1 = |\mathbf{r}_1| \quad (8)$$

$$r_2 = |\mathbf{r}_2| \quad (9)$$

$$r_{12} = |\mathbf{r}_1 - \mathbf{r}_2|, \quad (10)$$

and rewrite the Hamiltonian

$$\mathcal{H} = \mathcal{T}_0 + \mathcal{T}_{\text{cm}} + \mathcal{T}_{\text{mp}} + \mathcal{V}, \quad (11)$$

where

$$\mathcal{T}_0 = -\frac{1}{2\mu}(\nabla_{r_1}^2 + \nabla_{r_2}^2), \quad (12)$$

$$\mathcal{T}_{\text{cm}} = -\frac{1}{2(M + 2m)}\nabla_{\mathbf{R}}^2, \quad (13)$$

$$\mathcal{T}_{\text{mp}} = -\frac{1}{M}\nabla_{\mathbf{r}_1} \cdot \nabla_{\mathbf{r}_2}, \quad (14)$$

$$\mathcal{V} = -\frac{Z}{r_1} - \frac{Z}{r_2} + \frac{\alpha}{r_{12}}, \quad (15)$$

$\mu = mM/(M + m)$ is the reduced mass of the electron and nucleus, and $\nabla_{\mathbf{x}}$ is the gradient operator with respect to the vector \mathbf{x} .

In the center-of-mass frame \mathcal{T}_{cm} may be dropped bringing to six the number of nontrivial coordinates on which the wave function depends. Because $m \ll M$, the mass polarization term \mathcal{T}_{mp} is often ignored or treated perturbatively. While unnecessary for many methods including PS, we use the infinite nuclear mass approximation ($M = \infty$) to facilitate comparison with previous results. In units with $m = 1$ (atomic units) the Hamiltonian is

$$\mathcal{H} = -\frac{1}{2}(\nabla_{r_1}^2 + \nabla_{r_2}^2) - \frac{Z}{r_1} - \frac{Z}{r_2} + \frac{\alpha}{r_{12}}. \quad (16)$$

Atomic units are used throughout the rest of this article.

This operator is elliptic. All boundaries in physical space require specification of the function or its normal derivative or some combination of the two [73]. In the ideal problem, the physical boundary is at infinity where the wave function must be zero. The existence of the Coulomb potential's singular points at $r_1 = 0$, $r_2 = 0$, and $r_{12} = 0$ introduces complications in any formal and practical analysis. Before the exact nature of the Hermitian Hamiltonian operator and its spectrum was understood, Kato [74] showed that discrete eigenstates existed

for the specific case of helium. In later work Kato [75] showed that the wave function must be finite at the singular points (which is also true everywhere else) and that the first derivative of the wave function on the domain excluding the singular points is bounded. This result allows discontinuities in the first derivative at the singular points, called Kato cusps. Generally, higher derivatives are not bounded at the singular points.

In any numerical treatment of the Hamiltonian operator a decision must be made about how to handle the singular points. In a formal mathematical sense, quantities at the singularities are well defined only in the limit as one approaches the singularity. This creates an effective inner boundary about such points on which additional conditions on the function and its normal derivative may be specified. Such conditions are exploited to guarantee regularity in the limit that the excised region shrinks to a point. This article assumes that it is correct to excise such a point, either explicitly or implicitly.

III. COORDINATES AND THE HAMILTONIAN

The heliumlike atom is made of three particles: a nucleus and two electrons. Six coordinates are required to describe relative positions. Three coordinates describe the precise shape and size of the triangle with a particle at each vertex, and the other three describe the orientation of that triangle in space (often taken to be Euler angles). The wave function for S states is completely independent of the latter three [4]. For nonzero angular momentum one first expands the wave function in generalized spherical harmonics of the Euler angles. Only a finite number of terms are needed for a given total angular momentum and its z component, and the Schrödinger equation becomes a finite set of coupled partial differential equations for the remaining three variables (e.g., Refs. [76,77]).

Two useful sets of coordinates for the triangle are $\{r_1, r_2, r_{12}\}$ and $\{r_1, r_2, \theta_{12}\}$, where r_1 and r_2 are the proton-electron distances, r_{12} is the electron-electron distance, and θ_{12} is the angle between the vectors pointing to the two electrons. Four additional useful sets of coordinates $\{\rho \text{ or } x, \phi, C\}$ and $\{\rho \text{ or } x, \zeta, B\}$ are defined by

$$r_1 = \rho \cos \phi \quad (17)$$

$$r_2 = \rho \sin \phi \quad (18)$$

$$C = -\cos \theta_{12} \quad (19)$$

$$\sqrt{2} \sin \zeta = \sqrt{1 + C \sin 2\phi} \quad (20)$$

$$B = \frac{\cos 2\phi}{\sqrt{1 - C^2 \sin^2 2\phi}} \quad (21)$$

$$x = \frac{1 - \rho}{1 + \rho}. \quad (22)$$

The ranges of these variables are given by:

$$\begin{aligned} 0 &\leq r_1, r_2, \rho < \infty \\ |r_1 - r_2| &\leq r_{12} \leq r_1 + r_2 \\ 0 &\leq \theta_{12} \leq \pi \\ 0 &\leq \phi, \zeta \leq \pi/2 \\ -1 &\leq x, C, B \leq 1. \end{aligned} \quad (23)$$

The coordinate x maps the semi-infinite domain to a finite domain.² This simple choice works well because the wave function is exponentially small at large ρ for bound states which are the topic of interest here.

After integrating over the Euler angles the volume elements are

$$\int d^3\mathbf{r}_1 d^3\mathbf{r}_2 = 2\pi^2 \begin{cases} 4 \int r_1 r_2 r_{12} dr_1 dr_2 dr_{12} \\ 4 \int r_1^2 r_2^2 \sin \theta_{12} dr_1 dr_2 d\theta_{12} \\ \int \rho^5 \sin^2 2\phi d\rho d\phi dC \\ 2 \int \rho^5 \sin^2 2\zeta d\rho d\zeta dB \\ 2 \int \frac{(1-x)^5}{(1+x)^7} \sin^2 2\phi dx d\phi dC \\ 4 \int \frac{(1-x)^5}{(1+x)^7} \sin^2 2\zeta dx d\zeta dB. \end{cases} \quad (24)$$

The Hamiltonian for S states can be written in hyperspherical coordinates as:

$$\mathcal{H} = \mathcal{T}_\rho + \rho^{-2}(\mathcal{T}_\phi + \csc^2 2\phi \mathcal{T}_C) + \rho^{-1}\mathcal{U} \quad (25)$$

$$= \mathcal{T}_\rho + \rho^{-2}(\mathcal{T}_\zeta + \csc^2 2\zeta \mathcal{T}_B) + \rho^{-1}\mathcal{U}, \quad (26)$$

where

$$\mathcal{T}_\rho = -\frac{1}{2}\partial_{\rho\rho} - \frac{5}{2\rho}\partial_\rho \quad (27)$$

$$= -\frac{(1+x)^4}{8}\partial_{xx} + \frac{(1+x)^3(4+x)}{4(1-x)}\partial_x \quad (28)$$

$$\mathcal{T}_\phi = -\left(\frac{1}{2}\partial_{\phi\phi} + 2\cot 2\phi\partial_\phi\right) \quad (29)$$

$$\mathcal{T}_C = -2[(1-C^2)\partial_{CC} - 2C\partial_C] \quad (30)$$

$$\mathcal{T}_\zeta = -\left(\frac{1}{2}\partial_{\zeta\zeta} + 2\cot 2\zeta\partial_\zeta\right) \quad (31)$$

$$\mathcal{T}_B = -2[(1-B^2)\partial_{BB} - 2B\partial_B] \quad (32)$$

$$\mathcal{U} = \frac{\alpha}{\sigma[C, \phi]} - Z \csc \phi - Z \sec \phi \quad (33)$$

$$= \frac{\alpha}{\sqrt{2}\sin \zeta} - \frac{Z\sqrt{2}}{\sigma[B, \zeta]} - \frac{Z\sqrt{2}}{\sigma[-B, \zeta]}, \quad (34)$$

and

$$\sigma[x, y] = \sqrt{1+x}\sin 2y. \quad (35)$$

IV. THE SINGULAR POINTS IN THE HAMILTONIAN

PS methods are very sensitive to discontinuous derivatives of any order. If such discontinuities exist, the method loses its exponential convergence and artificial oscillations may occur. The wave function has discontinuities only at the singular points which thus require special attention. Myers *et al.* [78] discuss these singularities in detail. Here we reproduce some of their discussion for completeness.

²One can introduce a free parameter L by defining $x = (1 - \rho/L)/(1 + \rho/L)$ and vary L to optimize convergence but doing this led to only slight improvements. This finding is in agreement with Boyd *et al.* [63], who showed that L has a small effect for the hydrogen atom when using a Chebyshev basis.

A. Two-particle coalescences

There exist three lines corresponding to two-particle coalescences: two for the proton and each electron at $\phi = 0$ and $\phi = \pi/2$ and one for the two electrons at $\zeta = 0$. Only one of the proton-electron coalescence lines need appear in the numerical domain which takes advantage of the explicit symmetry of the spatial part of the wave function about $\phi = \pi/4$.

Kato [79] analyzed the discontinuity in the derivative of a wave function at two particle coalescence points and showed that

$$\left. \frac{\partial \hat{\psi}}{\partial r} \right|_{r=0} = \mu_{ij} q_i q_j \psi(r=0), \quad (36)$$

where ψ is the wave function, r is the particle-particle distance, $\hat{\psi}$ is the limit of the average value of the wave function on a sphere centered at $r = 0$ as its radius shrinks to zero, μ_{ij} is the reduced mass of the two particles, and q_i and q_j are the charges of the two particles.

Pack and Byers Brown [80] extended the analysis to show that the wave function could be expanded in terms of hydrogenic solutions.

$$\psi = \sum_{lm} a_{lm} r^l Y_l^m[\theta, \phi] \left(1 + \frac{q_i q_j \mu_{ij}}{l+1} r + O[r^2]\right), \quad (37)$$

where $l \geq 0$, $|m| \leq l$, a_{lm} is an expansion coefficient, θ and ϕ are the usual spherical angles giving the orientation of the two particles, and Y_l^m is the usual spherical harmonic.

These results describe the regularity required at the Coulomb singularities. There are three practical approaches to making sure the solution has the appropriate behavior.

1. Behavioral

Assume that local solutions to the Schrödinger equation that fail to satisfy Eqs. (36) and (37) are not analytic; assume that the expansion (cardinal functions) employed in the numerical treatment is incapable of representing this nonanalytic behavior. Granted these assumptions, all numerical solutions will automatically be regular at the point in question.³ According to Boyd [3], in many contexts this approach is sufficient. If the solutions that do not satisfy Eqs. (36) and (37) have only weakly singular behavior, the convergence rate may be slow.

2. Regularity

Replace the Hamiltonian at the singular points with the Kato cusp conditions without otherwise altering the domain. The cusp conditions are

$$\left. \frac{\partial \hat{\psi}}{\partial \phi} \right|_{\phi=0} = -Z\rho\psi(\phi=0) \quad (38)$$

³Because it is impossible to work where the potential diverges, the grid must be designed to exclude the point in question. The fact the grid does not contain the point is not a requirement of the behavioral approach.

$$\left. \frac{\partial \hat{\psi}}{\partial \phi} \right|_{\phi=\pi/2} = Z\rho\psi\left(\phi = \frac{\pi}{2}\right) \quad (39)$$

$$\left. \frac{\partial \hat{\psi}}{\partial \zeta} \right|_{\zeta=0} = \frac{\alpha\rho}{2}\psi(\zeta = 0) \quad (40)$$

or

$$\psi(\phi = 0) = 0 \quad (41)$$

$$\psi\left(\phi = \frac{\pi}{2}\right) = 0 \quad (42)$$

$$\psi(\zeta = 0) = 0, \quad (43)$$

where these two sets are mixed and matched while preserving the appropriate symmetry or antisymmetry. The choice depends on precisely which state one wishes to calculate.

3. Excision

Excise a small sphere around the singular points and impose boundary conditions on its surface that yield the correct behavior at the singularity as the sphere shrinks. From Eq. (37)

$$\psi = \sum_l b_l \rho^l \phi^l P_l[C] \left(1 - \frac{Z\rho\phi}{l+1} + O[\rho^2\phi^2]\right) \quad (44)$$

$$\psi = \sum_l c_l \rho^l \tilde{\phi}^l P_l[C] \left(1 - \frac{Z\rho\tilde{\phi}}{l+1} + O[\rho^2\tilde{\phi}^2]\right) \quad (45)$$

$$\psi = \sum_l d_l \rho^l \zeta^l P_l[B] \left(1 + \frac{\alpha\rho\zeta\sqrt{2}}{2(l+1)} + O[\rho^2\zeta^2]\right), \quad (46)$$

where $\tilde{\phi} = \pi/2 - \phi$, P_l is a Legendre polynomial of order l , and b_l , c_l , and d_l are unknown constants. Define

$$\xi_l = \int_{-1}^1 \psi P_l[C] dC \quad (47)$$

$$\chi_l = \int_{-1}^1 \psi P_l[B] dB, \quad (48)$$

and write the conditions as

$$0 = \phi \frac{\partial \xi_l}{\partial \phi} + \left(-l + \rho\phi \frac{Z}{l+1}\right) \xi_l \quad (49)$$

$$= -\tilde{\phi} \frac{\partial \xi_l}{\partial \phi} + \left(-l + \rho\tilde{\phi} \frac{Z}{l+1}\right) \xi_l \quad (50)$$

$$= \zeta \frac{\partial \chi_l}{\partial \zeta} - \left(l + \frac{\alpha\rho\zeta\sqrt{2}}{2(l+1)}\right) \chi_l. \quad (51)$$

These conditions become exact as the excised volume shrinks to a point. For PS methods the volume should be reduced exponentially with increasing resolution. The changes do not increase the computational cost but may adversely affect the condition number of the matrix.

The difficulty of implementation increases with number on the list.

B. Three particle coalescence

The potential is also singular when all three particles collide (i.e., when the hyperradius, ρ goes to zero). The behavior of the wave function about this point is much less well understood than two-particle coalescences and cannot be handled in the same way. Instead of simply having a discontinuity in the wave function's first derivative (the value of which is finite on both sides of the singularity), the second derivative grows logarithmically near $\rho = 0$. Bartlett [26] was the first to show that a simple Frobenius type expansion in powers of ρ about $\rho = 0$ fails at second order on account of the electron-electron interaction. He suggested that logarithmic terms exist in the exact solution of helium. Fock [81,82] introduced an expansion of the form

$$\psi = \sum_{n=0}^{\infty} \sum_{m=0}^{\lfloor n/2 \rfloor} e_{nm} \rho^n (\log \rho)^m, \quad (52)$$

where e_{nm} are two dimensional functions of the hyperangles $\{\phi, C\}$ or $\{\zeta, B\}$ determined through the recursive relationship

$$\begin{aligned} [n(n+4) + \Delta]e_{nm} &= 2Ve_{n-1,m} - 2Ee_{n-2,m} \\ &\quad - 2(n+2)(m+1)e_{n,m+1} \\ &\quad - (m+1)(m+2)e_{n,m+2}, \end{aligned} \quad (53)$$

and Δ is the two-dimensional Laplacian over the hyperangles. All e_{nm} with $n \leq 2$ are known analytically plus a few additional terms with higher n [83–86]. Morgan proved that the series is convergent everywhere [87], and it has been shown that variational calculations converge faster when a single power of a logarithm is included in the basis [7].⁴

Again, there are three basic strategies for a numerical scheme:

1. Behavioral

Do nothing special and rely on the regularity of the cardinal functions. This is an imperfect approach since the exact wave function has unbounded second derivatives as $\rho \rightarrow 0$. If the basis set can only represent regular behavior as discussed in the case of two-particle coalescence it will not produce the exact solution. However, since the volume element scales as $\rho^5 d\rho$ such inexactness may have negligible effect on observables calculated from the wave function.

2. Regularity

Impose a regularity-like condition at the singular point. For the ground state (and many other S states), the first-order solution [81,82] to the Fock Eqs. (53) is

$$e_{00} = c \quad (54)$$

$$e_{10} = c \left\{ -Z(\cos \phi + \sin \phi) + \frac{\alpha}{2} \sigma[C, \phi] \right\}, \quad (55)$$

where c is a constant given by the normalization. These solutions imply either

$$\begin{aligned} \partial_\rho \psi|_{\rho=0} &= \left\{ -Z(\cos \phi + \sin \phi) + \frac{\alpha}{2} \sigma[C, \phi] \right\} \\ &\quad \times \psi(\rho = 0), \end{aligned} \quad (56)$$

⁴Curiously, higher powers of the logarithm do not seem to improve the convergence rate of variational calculations [28].

which is valid for the ground state, or

$$\psi(\rho = 0) = 0. \tag{57}$$

Note that this regularity-like condition says nothing about the second derivatives. For the same reasons as above this method can never give the exact solution at $\rho = 0$.

3. Excision

Excise a small domain with $\rho < \rho_{\min}$, where ρ_{\min} is the cutoff. A boundary condition can be calculated on this inner surface by solving Eq. (53) to relate the wave function and normal derivative on the surface.⁵ As the resolution increases, more terms must be calculated so that the truncation error in the Fock expansion equals the error due to having finite resolution in the numerical calculation. The basis set expansion in the bulk remains completely regular. While exact, the method is complicated and will be pursued at a later time.

C. Infinite separation

The domain of the ideal problem extends to infinity. The bound-state wave functions fall off exponentially. The outer boundary condition must be approximated in the numerical method. There are several approaches.

1. Behavioral

Rely on the regularity of the cardinal functions to exclude exponentially growing solutions as $\rho \rightarrow \infty$. One must map the semi-infinite domain to a finite one to use Chebyshev collocation points or work with semi-infinite functions like Laguerre polynomials.

2. Regularity

Again map the domain to a finite one but replace the Schrödinger equation at $\rho = \infty$ by

$$\psi(\rho = \infty) = 0. \tag{58}$$

Note that if one includes the endpoints using the behavioral method, this method is effectively the same as the behavioral condition because the Schrödinger equation reduces to $E\psi = 0$ at $x = -1$ ($\rho = \infty$).

3. Excision

Excise the region with $\rho > \rho_{\max}$ where ρ_{\max} is the cutoff and impose a suitable boundary condition. As in the three-particle coalescence, one may develop a more and more accurate representation at fixed ρ_{\max} and/or an approximate condition at increasing ρ_{\max} . It is easiest to set

$$\psi(\rho = \rho_{\max}) = 0 \tag{59}$$

or

$$\left. \frac{\partial \psi}{\partial \rho} \right|_{\rho=\rho_{\max}} = 0 \tag{60}$$

⁵The boundary condition is not known in analytic form (except at low order) but must be inferred by a numerical technique. Solutions to Eq. (53) can be found numerically with similar techniques as employed here for the full three-dimensional problem.

and vary ρ_{\max} , which is what is done in this article when using this method. In a PS numerical scheme one should vary $\rho_{\max} \propto n^{1/2}$ for large n where n is the radial resolution (see Appendix A).

D. Collinearity (B or $C = \pm 1$)

The coefficients multiplying the second derivatives with respect to B and C at $B, C = \pm 1$ go to zero. In ordinary differential equations this allows irregular solutions that behave as linear combinations of Legendre functions of the second kind. Regularity of the cardinal functions excludes such solutions. Since the Schrödinger equation at these points contains no infinities it does not matter if the grid includes these points. The partial differential equation is parabolic along this boundary. So no boundary conditions or regularity conditions need to be given.

V. THE PSEUDOSPECTRAL METHOD

Boyd [3], Fornberg [55], Pfeiffer *et al.* [59], and the third edition of *Numerical Recipes* [56] cover the PS method in detail. A brief review of some aspects pertinent to our work follows.

The main advantage of this method is that it provides exponentially fast convergence for smooth solutions. Unlike finite difference and finite element algorithms, all derivatives are calculated to higher and higher order with increasing resolution.

It is also noteworthy that the grid points are clustered more closely near the boundary of a domain than in its center. With this arrangement the representation of a function and its derivative is more uniformly accurate across the whole domain than is possible using an equal number of equidistant points. Finite difference and finite element methods typically use an equal-spaced grid and the derivatives are less accurate at the edge than at the center.

Let n_d be the number of coordinate dimensions and N_i the resolution in the i th dimension. The differential equation is enforced at $n_i = \prod_{i=1}^{n_d} N_i$ collocation or grid points chosen to be the roots or extrema of a Jacobi polynomial of order N_i in each dimension. Boyd's recommendation that one use Chebyshev polynomials to generate the grid points in lieu of special circumstances is followed here [3].

The derivatives in the i th direction are calculated to N_i^{th} order in terms of the function values at the collocation points. To illustrate this it is useful to define the cardinal functions:

$$C_j^N[x] = \prod_{\substack{i=1 \\ i \neq j}}^N \frac{x - x^i}{x^j - x^i}, \tag{61}$$

where the x^i 's are the collocation points and i and j are superscripts not exponents. These functions have the property that

$$C_j^N[x^i] = \delta_j^i. \tag{62}$$

The PS representation of a function at an arbitrary n_d -dimensional position (x_1, \dots, x_{n_d}) is expanded as

$$\psi \approx \psi_{N_1, \dots, N_{n_d}} = \psi^{j_1, \dots, j_{n_d}} F_{j_1, \dots, j_{n_d}}^{N_1, \dots, N_{n_d}} [x_1, \dots, x_{n_d}], \tag{63}$$

(using the Einstein summation convention) in terms of its grid values and the cardinal functions

$$\psi^{j_1, \dots, j_{n_d}} = \psi_{N_1, \dots, N_{n_d}} [x_1^{j_1}, \dots, x_{n_d}^{j_{n_d}}] \quad (64)$$

$$F_{j_1, \dots, j_{n_d}}^{N_1, \dots, N_{n_d}} = \prod_{i=1}^{n_d} C_{j_i}^{N_i} [x_i]. \quad (65)$$

Such an expansion is equivalent (up to an exponentially small error for smooth functions) to a spectral one,

$$\psi = s^{j_1, \dots, j_{n_d}} G_{j_1, \dots, j_{n_d}} [x_1, \dots, x_{n_d}], \quad (66)$$

where

$$G_j = \prod_{i=1}^{n_d} u_{j_i} [x_i] \quad (67)$$

$$s^{j_1, \dots, j_{n_d}} = \int \psi G_j \prod_{i=1}^{n_d} w [x_i] dx_i \quad (68)$$

$$\approx \psi^{i_1, \dots, i_{n_d}} G_j [x_1^{i_1}, \dots, x_{n_d}^{i_{n_d}}] \prod_{k=1}^{n_d} v_{i_k}, \quad (69)$$

\mathbf{j} means j_1, \dots, j_{n_d} , u_{j_i} are orthonormal polynomials chosen here to be Chebyshev polynomials, w is the weight function over which they are orthonormal, and v_{i_k} are the corresponding quadrature weights. Note, the collocation points are also quadrature points which allow exponential convergence of the quadrature. Derivatives of ψ are approximated by differentiating Eq. (63). To this end, it is useful to introduce differentiation matrices,

$$(D_N)_j^i = \partial_x C_j^N [x] |_{x=x^i}. \quad (70)$$

This method is readily applied to linear eigenvalue problems as arise from the Schrödinger equation⁶

$$(\mathcal{H} - E)\psi = 0, \quad (71)$$

where \mathcal{H} is the Hamiltonian operator, ψ is the wave function, and E is the energy eigenvalue. Discretizing on the grid gives the tensor equation

$$H_{j_1, j_2, \dots, j_{n_d}}^{i_1, i_2, \dots, i_{n_d}} \psi_{j_1, j_2, \dots, j_{n_d}} = E \psi_{i_1, i_2, \dots, i_{n_d}}, \quad (72)$$

where

$$H_{j_1, j_2, \dots, j_{n_d}}^{i_1, i_2, \dots, i_{n_d}} = \mathcal{H} F_{j_1, j_2, \dots, j_{n_d}} [x_1^{i_1}, x_2^{i_2}, \dots, x_{n_d}^{i_{n_d}}]. \quad (73)$$

Unlike finite difference methods, the tensor $H_{j_1, j_2, \dots, j_{n_d}}^{i_1, i_2, \dots, i_{n_d}}$ is dense. Write this as $H_{l(j_1, j_2, \dots, j_{n_d})}^{k(i_1, i_2, \dots, i_{n_d})}$ or for short H_l^k , where k and l are one-to-one functions mapping the set of n_d indices to the lowest n_t positive integers. This recasts the tensor as a large matrix so that standard matrix methods can be employed.

One way to carry out the mapping employs the Kronecker product as follows. If \mathcal{H} is given by

$$\mathcal{H} = \sum_{i_1, \dots, i_{n_d}} f_{i_1, \dots, i_{n_d}} [x_1, \dots, x_{n_d}] (\partial_{x_1})^{i_1} \dots (\partial_{x_{n_d}})^{i_{n_d}}, \quad (74)$$

where $f_{i_1, \dots, i_{n_d}}$ is a function coefficient, then the matrix, H is given by

$$H_l^k = \sum_{i_1, \dots, i_{n_d}} f_{i_1, \dots, i_{n_d}} [\mathbf{x}^k] \left(\bigotimes_{j=1}^{n_d} (D_{N_j})^{i_j} \right)_l, \quad (75)$$

where \mathbf{x}^k is the n_d -dimensional vector of coordinates with indices that map to k , N_j is the number of grid points in the j^{th} direction, i_j is an exponent, and D_{N_j} is the differential matrix based on N_j points.

VI. PSEUDOSPECTRAL CONVERGENCE FOR NONSMOOTH FUNCTIONS

To make appropriate design algorithmic choices it is important to investigate how the PS method handles nonsmooth behavior of solutions. This section explores the convergence of truncated cardinal function expansions to cusps and logarithmic terms and then employs a toy model that illustrates how the triple coalescence is expected to influence the numerical results.

A. Kato cusps

Consider the ground state of the hydrogen atom with wave function

$$\psi = e^{-r} = e^{-\sqrt{x^2+y^2+z^2}}. \quad (76)$$

In Cartesian coordinates, there is a discontinuity in the first derivative at the origin,

$$\lim_{x \rightarrow 0^+} \frac{\partial \psi}{\partial x} \Big|_{y=z=0} \neq \lim_{x \rightarrow 0^-} \frac{\partial \psi}{\partial x} \Big|_{y=z=0}. \quad (77)$$

In spherical coordinates no discontinuity exists for $r \geq 0$. All the derivatives at $r = 0$ are well defined and a PS code has no problem exponentially converging toward the correct answer. The essence of this observation can be seen by considering the one-dimensional exponential functions

$$g_1[x] = e^{-|x|} \quad (78)$$

$$g_2[x] = e^{-(x+1)}, \quad (79)$$

on the domain $-1 \leq x \leq 1$ with weight x^2 (analogous to the three dimensional hydrogen atom). As a measure of error between the function f and its cardinal expansion truncated at order n define

$$\delta_{\text{RMS}}^N[f] = \sqrt{\int_{-1}^1 x^2 \left(f[x] - \sum_{i=1}^N C_i^N [x] f[x^i] \right)^2 dx}. \quad (80)$$

Figure 1 compares $\delta_{\text{RMS}}^n[g_1]$ to $\delta_{\text{RMS}}^n[g_2]$ as a function of n . Evidently the cusp is poorly represented compared to the smooth function at a given n . The PS representation of the cusp converges algebraically while the representation of the smooth function converges supergeometrically (see Appendix B for fits).

The basic strategy in more complicated problems is to adopt a coordinate system with a radial-like coordinate at each cusp. For two-electron atoms no global coordinate system exists with the desired property at each of the three separate two-particle coalescences. This article uses three individual but

⁶Linearity is not required for the PS method.

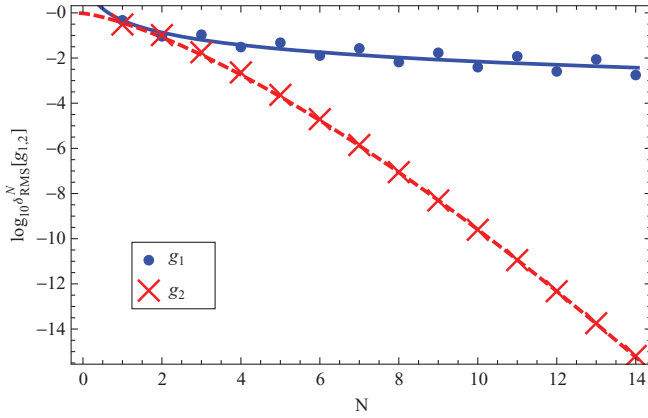


FIG. 1. (Color online) The logarithm base 10 of $\delta_{\text{RMS}}^N[g_1]$ (blue circles) and $\delta_{\text{RMS}}^N[g_2]$ (red crosses) with solid blue and dashed red fits, respectively. See Appendix B for fitting functions.

overlapping domains to guarantee appropriate treatment near each coalescence point.

B. Logarithmic terms

Consider the one-dimensional function

$$f[x] = \left\{ 1 + \frac{1}{2}\alpha\rho[x]^2 \log[\rho[x]] \right\} e^{-\rho[x]}, \quad (81)$$

where

$$\rho[x] = \frac{1-x}{1+x}. \quad (82)$$

Here $\rho \in [0, \infty)$, $x \in [-1, 1]$ and f are analogous to the hyperspherical radius, its algebraic transformation and the heliumlike wave function ψ , respectively. As in the full three-dimensional problem, the presence or absence of the logarithmic terms is controlled by α , which can be set to 0 or 1.

There are two types of errors considered here: interpolation error and operator error. These are different sorts of error, but qualitative features (e.g., exponential or algebraic convergence) are expected to be the same.

1. Interpolation error

The pointwise error between f and its truncated expansion is

$$\Delta f = f[x] - \sum_{i=1}^N C_i^N[x] f[x^i], \quad (83)$$

where x^i refers to the i th grid point.

Figure 2 shows that the behavior of Δf at three different values of ρ . For each value the apparent rate of convergence starts out exponential before becoming algebraic at large N . The algebraic convergence known with the highest accuracy in Fig. 2 is for $\rho = 10^{-6}$, which asymptotically goes as $1/N^{3.82 \pm 0.09}$ (see Appendix B). This algebraic behavior is expected when trying to represent a nonanalytic function ($\log[\rho]$) with an analytic basis. Such behavior disappears if α is set to zero.

The onset of algebraic convergence varies from $N \approx 40$ to $N \approx 80$ as ρ , moving away from the singularity, increases by

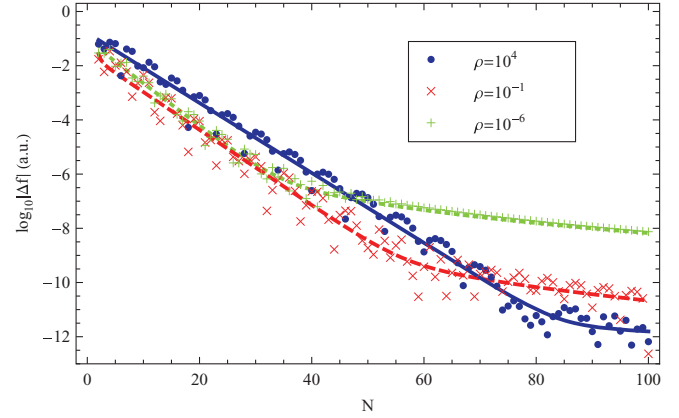


FIG. 2. (Color online) The logarithm base 10 of the error in $f[x]$ using cardinal functions at $\rho = 10^{-6}$ (green pluses), $\rho = 10^{-1}$ (red crosses), and $\rho = 10^4$ (blue circles) with solid blue, dashed red, and dotted green fits, respectively. See Appendix B for fitting functions and method.

10 orders of magnitude. The error at the transition is $< 10^{-6}$. Typically, energy errors vary as the square of wave function errors and would already be very small compared to relativistic corrections. This calculation shows that it is possible to get precise values with apparent exponential convergence before reaching the asymptotic algebraic regime. As a practical matter, one may never reach the latter limit.

2. Operator error

In order to estimate the error in the eigenvalue, it would help to have a one-dimensional toy eigenvalue problem with an eigenfunction similar to the function in Eq. (81). It is impossible to construct a one-dimensional eigenvalue problem with solutions that have logarithmic singularities without explicitly introducing such singularities into the differential operator. So here a more limited test problem is used. Instead of solving for an eigenvalue, the error in the operator is measured. This would contribute to the eigenvalue error along with the error in the wave function.

Let $\Delta \mathcal{H}$ be the difference between the true Hamiltonian and the Hamiltonian constructed from PS differentiation matrices. The associated energy error is $\langle \psi | \Delta \mathcal{H} | \psi \rangle$. The aim is to construct an analog of the integrand of the energy error and use it to assess pointwise and integral errors.

Construct a differential operator \mathcal{D} similar to the full Hamiltonian \mathcal{H} [see Eq. (25)] but in terms of the coordinate x ,

$$\mathcal{D} = p_2[x] \partial_{xx} + p_1[x] \partial_x + p_0[x], \quad (84)$$

where

$$p_2[x] = -\frac{(1+x)^4}{8} \quad (85)$$

$$p_1[x] = \frac{(1+x)^3}{4} \left(\frac{4+x}{1-x} \right) \quad (86)$$

$$p_0[x] = -\frac{1}{\rho[x]}. \quad (87)$$

Note, the first two terms are identical to the operator \mathcal{T}_ρ and the last term is a Coulomb potential.

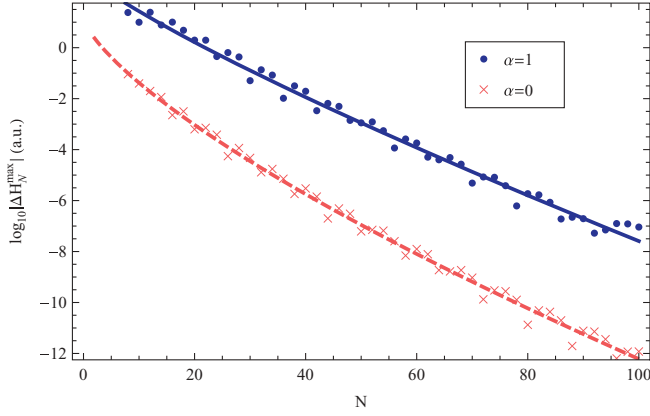


FIG. 3. (Color online) The logarithm base 10 of the maximum error of a pseudospectral matrix. The dark blue circles are for $\alpha = 1$ and the light red crosses for $\alpha = 0$ with solid blue and dashed red fits, respectively. See Appendix B for fitting functions and method.

The corresponding matrix operator is

$$(d_N)_j^i = p_2[x^i](D_N)_k^i(D_N)_j^k + p_1[x^i](D_N)_j^i + p_0[x^i]\delta_j^i, \quad (88)$$

where Einstein's summation convention is used and δ_j^i is the Kronecker delta function. The pointwise error on the grid and its maximum are

$$(\Delta H_N)^i = w[x^i] \left((Df)[x^i] - \sum_j (d_N)_j^i f[x^j] \right) \quad (89)$$

$$\Delta H_N^{\max} = \max_i |(\Delta H_N)^i|, \quad (90)$$

where

$$w[x] = \frac{(1-x)^5}{(1+x)^7} f[x] \quad (91)$$

The factor $(1-x)^5/(1+x)^7$ comes from the Jacobian.

Figure 3 shows ΔH_N^{\max} , the maximum error anywhere on the grid, as a function of n for $\alpha = 0$ and $\alpha = 1$. The decrease appears to be exponential, not unanticipated when $\alpha = 0$ but perhaps a surprise for $\alpha = 1$. The slopes of the two curves are roughly the same and the offset is due to the variation of the magnitude of f with α . An explanation is immediately suggested by Fig. 4 which shows the error at the grid point closest to the singularity $(\Delta H_N)^{i^*}$ (here i^* refers to that point). The data for $\alpha = 1$ is well fit by an algebraic rate of convergence $(1/N^{10.36 \pm 0.08})$ at large N while $\alpha = 0$ has an approximately exponential fall-off (the convergence is subgeometric because the calculation is done on a semi-infinite domain). The log term *does* spoil the method's exponential convergence. Assuming that the effect is greatest at $i = i^*$, the maximum error is dominated by the log term when N is greater than about 200 and the error is *very* small. This is exponential convergence “for all practical purposes.”

C. Conclusion

For the interpolation and operator errors, the logarithmic term does not slow convergence unless one is at high resolution or interested in small values of ρ . For those cases, one would

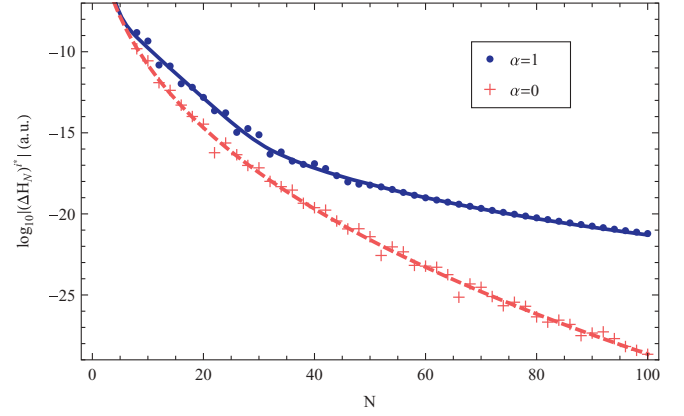


FIG. 4. (Color online) The logarithm base 10 of the error of a pseudospectral matrix near the singularity. The dark blue circles are for $\alpha = 1$ and the light red pluses for $\alpha = 0$ with solid blue and dashed red fits, respectively. See Appendix B for fitting functions and method.

need to apply the excision method about the triple coalescence point in order to retain exponential convergence. For most applications the level of precision needed is obtained before the algebraic behavior becomes apparent.

VII. NUMERICAL DOMAINS AND COLLOCATION POINTS

Because the two electrons are identical particles the full wave function is antisymmetric. In the ground state, the spins are antisymmetric and the spatial part is symmetric. The spatial domain may be taken as $\phi < \pi/4$ and $B > 0$. The complete numerical domain is

$$\begin{aligned} D_0 : -1 \leq x \leq 1 \quad 0 \leq \phi \leq \frac{\pi}{4} \quad -1 \leq C \leq 1 \\ \text{or} \\ D_0 : -1 \leq x \leq 1 \quad 0 \leq \zeta \leq \frac{\pi}{2} \quad 0 \leq B \leq 1. \end{aligned} \quad (92)$$

A single domain does not allow the proper treatment of the two-particle coalescences. Therefore, introduce three subdomains to cover D_0 using two different sets of variables:

$$\begin{aligned} D_1 : -1 \leq x \leq 1 \quad 0 \leq \phi \leq \frac{1}{2} \quad -1 \leq C \leq 1 \\ D_2 : -1 \leq x \leq 1 \quad \frac{1}{2} \leq \phi \leq \frac{\pi}{4} \quad -\frac{2}{3} \leq C \leq 1 \\ D_3 : -1 \leq x \leq 1 \quad 0 \leq \zeta \leq \frac{1}{2} \quad 0 \leq B \leq 1. \end{aligned} \quad (93)$$

For calculations done on a finite domain, the condition $-1 \leq x \leq 1$ is replaced by $0 \leq \rho \leq \rho_{\max}$. Cross sections of these domains at fixed ρ are shown in Fig. 5. An electron-proton singularity lies in D_1 , while the electron-electron singularity lies in D_3 . The radial-like coordinates in D_1 (ϕ) and D_3 (ζ) accommodate the cusps just like the usual radial coordinate does in the hydrogen atom. D_2 fills in the remaining volume. All three domains have boundaries that touch the triple coalescence point (not pictured).

Consideration of the electron-electron singularity shows why the single domain D_0 is inadequate. Byers Brown and White [88] showed that the wave function can be expanded in powers of r_{12} about $r_{12} = 0$. Using such a coordinate accurately treats the cusp away from the triple coalescence point. The expansion in powers of ζ is very similar [see Eq. (46)] or equivalently powers of

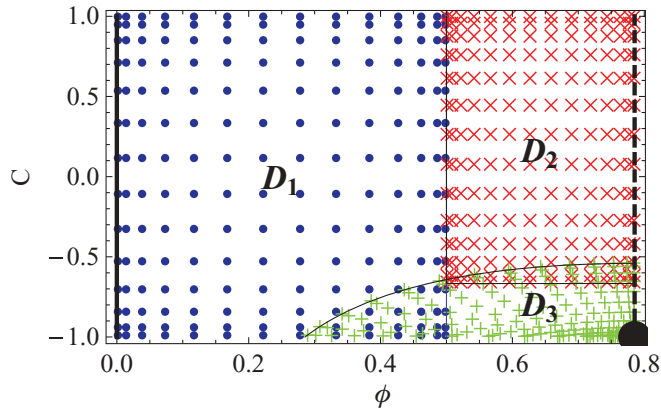


FIG. 5. (Color online) This is the arrangement of grid points of the three domains at a constant value of ρ in ϕ and C coordinates. Note that the point density becomes larger at the boundary of each subdomain and that no grid points sit on the Coulomb singularities. The blue circles, red crosses, and green pluses belong to domains D_1 , D_2 , and D_3 , respectively. D_1 and D_2 are rectangular domains, while D_3 has the curved boundary in ϕ , C coordinates but is rectangular in ζ , B coordinates. The electron-proton singularity occurs on the left side (solid line at $\phi = 0$). The entire line corresponds to one physical point. The electron-electron singularity occurs at the lower right-hand corner (solid disk at $\phi = \pi/4$, $C = -1$). A line of symmetry falls on the right side (dashed line at $\phi = \pi/4$ where $r_1 = r_2$).

$\sqrt{2} \sin \zeta = \sqrt{1 + C \sin 2\phi}$.⁷ Re-expanding in ϕ and C coordinates gives derivatives of $\sqrt{1 + C \sin 2\phi}$ with respect to C and ϕ , terms that are either infinite or undefined at $\phi = \pi/4$ and $C = -1$. This is why the PS method fails to converge rapidly using D_0 alone.

Within each domain, grid points are set as follows. Let the i th dimension extend from $x_{i,\min}$ to $x_{i,\max}$ and have N_i collocation points. These points are the roots or antinodes plus endpoints of the N_i^{th} order Chebyshev polynomial⁸ stretched to fit length $\Delta x_i = x_{i,\max} - x_{i,\min}$. The j th point (for $j = 1, 2, \dots, N_i$) of dimension i is

$$x_i^j = \frac{\Delta x_i}{2} (y_i^j + 1), \quad (94)$$

where

$$y_i^j = \cos \left[\frac{(N_i - j + \lambda)\pi}{N_i} \right] \quad (95)$$

and λ is 0 or 1/2 for nodes or antinodes plus endpoints, respectively.⁹ In this article, nodes are generally used except when

⁷The radius of convergence of the Byers Brown and White expansion is unknown to the authors but is clearly invalid at $\rho = 0$, the location of the triple coalescence point. Here only the effect of the double coalescence point is being considered.

⁸When the excision method is used near the two-particle coalescence points, the nodes of Legendre polynomials are used in the B and C directions. This choice makes it easier to apply Eq. (49) with a simple quadrature.

⁹It is also possible to use the so-called Chebyshev-Randau points, which include one endpoint on one side of the domain but not the other.

explicit boundary conditions are needed at both endpoints, $x_{i,\min}$ and $x_{i,\max}$.

Potentially each dimension and domain could have its own N_i but in this article the x direction is set to be twice as large as the other two dimensions and all are varied in lockstep. That is, $\{N_x, N_C, N_\phi\} = \{2n, n, n\}$ in domains D_1 and D_2 and $\{N_x, N_B, N_\zeta\} = \{2n, n, n\}$ in domain D_3 . The total number of grid points is $n_t = 3 \times (2n \times n \times n) = 6n^3$ points. Twice as many points were used in the x dimension, an arbitrary choice but one motivated by the semi-infinite range of the hyperspherical coordinate and by the wave function's logarithmic dependence on the hyperspherical radius near the triple coalescence point.

VIII. BOUNDARY CONDITIONS

A. Internal boundary conditions

It is necessary to ensure continuity of the wave function and its normal derivative at internal boundaries. There are two ways in which the subdomains can touch: they can overlap or they can barely touch. For clarity, consider a one-dimensional problem with two domains. Let the first domain be domain 1 and the second be domain 2 with extrema $x_{1,\min} < x_{2,\min} \leq x_{1,\max} < x_{2,\max}$, where the 1 and 2 now refer to domain number. The first case corresponds to $x_{2,\min} < x_{1,\max}$ and the second to $x_{2,\min} = x_{1,\max} \equiv x_*$. For both cases, exactly two conditions are need to make the wave function and its derivative continuous. The simplest choice for the first case is

$$\psi_1[x_{1,\max}] = \psi_2[x_{1,\max}] \quad (96)$$

$$\psi_1[x_{2,\min}] = \psi_2[x_{2,\min}], \quad (97)$$

and for the second case is

$$\psi_1[x_*] = \psi_2[x_*] \quad (98)$$

$$\frac{d}{dx} \psi_1[x_*] = \frac{d}{dx} \psi_2[x_*]. \quad (99)$$

For multidimensional grids, the situation is analogous. The conditions are applied on surfaces and the derivatives are normal derivatives at the surface. On a discrete grid, a finite number of conditions are given which, in the limit of an infinitely fine mesh, would cover the entire surface. There is a great deal of freedom in the selection of the points but in this article the edge of a domain has one constant coordinate so there is a natural choice. Conditions are imposed at the points of the finite mesh formed by varying all the other coordinates (in general, these are not collocation points). In other words, the matching points lie at the intersection of the coordinate lines normal to the surface with the surface itself. The positions of the crosses in Figs. 6 and 7 illustrate where the matching occurs when the domains overlap and when they just touch.

For touching domains, the black and white crosses in Fig. 7 are used. Note that four (three) crosses are defined by the coordinate lines in D_2 (D_1). At the set of four crosses, function values are equated, and at the set of three crosses, normal derivatives are equated. In general, function values (derivatives) are equated at points stemming from the subdomain with a greater (lesser) density of points along the boundary.

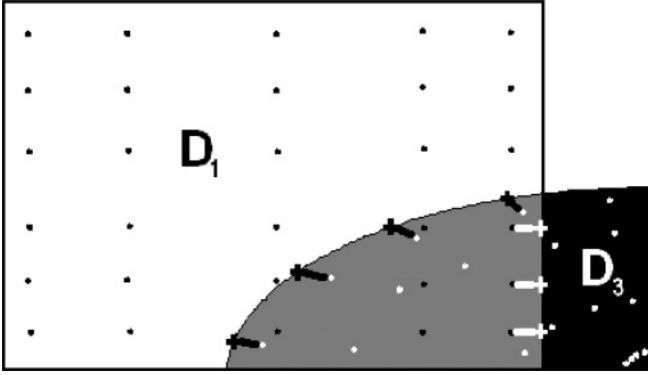


FIG. 6. The intersection (gray) of domains D_1 (white) with black grid points and D_3 (black) with white grid points. The boundary points are depicted as black and white crosses and are connected via black and white lines to the grid points that they replace.

For overlapping domains, the function values are equated at the black and white crosses in Fig. 6 which lie on two separate surfaces. The points are selected in a manner similar to that of touching domains, i.e., in terms of the intersection of the coordinate lines in D_1 and D_3 with the surface. In all cases, values and derivatives at all points are calculated using Eq. (63) and are ultimately linear combinations of the grid point values.

B. Symmetry and regularity conditions

For this problem there are two types of boundary conditions on the boundary of the numerical domain: the symmetry condition from electron exchange and the regularity conditions imposed near singular points.

The symmetry condition is related to the total spin of the two electrons, S . If $S = 0$ ($S = 1$) the wave function is symmetric (antisymmetric) about $\phi = \pi/4$ or $B = 0$ and the normal derivative (value) of the wave function is equal to zero. This condition is enforced at all the points on the boundary that have the same ρ and C coordinates as grid points in D_2 or the same ρ and ζ coordinates in D_3 . This gives $2 \times 2n \times n = 4n^2$ boundary conditions.

Regularity conditions are imposed as boundary conditions at four two-dimensional surfaces: $\rho = 0$, $\rho = \infty$, $\phi = 0$, and

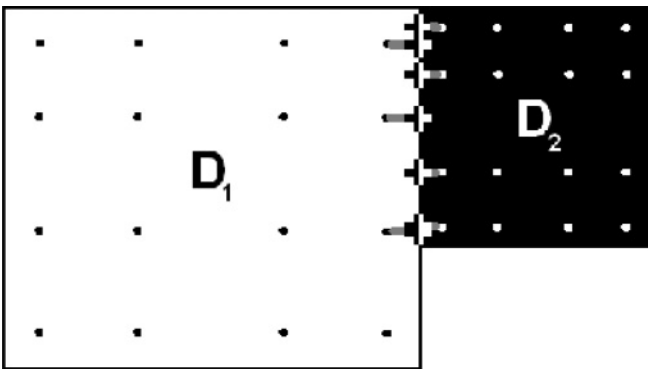


FIG. 7. Barely touching domains D_1 (white) with black grid points and D_2 (black) with white grid points. The boundary points are depicted as black and white crosses and are connected via gray lines to the grid points that they replace.

$\zeta = 0$. These are similar in form to the symmetry condition except involve linear combinations of derivative and value. Depending on which type of conditions are given at singular points (behavioral versus regularity or excision) are used, there are 0 to $10n^2$ conditions. These conditions replace an equal number of equations. The particular equation replaced is the one that stems from enforcement of the discretized Schrödinger equation at the collocation point nearest to the boundary at which the condition applies.

The most complicated type of boundary condition arises when a region is excised about a two-particle coalescence. First, one must project out terms proportional to each Legendre polynomial by performing an integral over C or B . This can be done by quadrature over the grid points in those dimensions. For example, Eq. (47) turns into

$$\xi_l[\rho^i, \phi^j] = \sum_k w_k P_l[C^k] \psi[\rho^i, \phi^j, C^k], \quad (100)$$

where w_k are the quadrature weights. Then Eq. (49) becomes for $j = 1$ (the excision boundary)

$$0 = \left[\phi^j (D_{N_\phi})_k^j + \left(-l + \frac{\rho^i \phi^j Z}{l+1} \right) \delta_k^j \right] \xi_l[\rho^i, \phi^k], \quad (101)$$

which is $N_\rho N_C$ conditions ($0 \leq l \leq N_C - 1$ and $1 \leq i \leq N_\rho$).

C. Incorporating boundary conditions into the matrix problem

All of the above boundary conditions are expressed as a linear combination of the function values at the grid points equal zero. In matrix form

$$n_b \{ \underbrace{(B_1 B_2)}_{n_b + n_i} \begin{pmatrix} \psi_1 \\ \psi_2 \end{pmatrix} \}_{n_i} = 0, \quad (102)$$

where ψ_1 (ψ_2) is a vector of the n_b (n_i) wave function values at all the boundary (interior) points, the boundary condition matrix has been broken into an n_b by n_b matrix B_1 and an n_b by n_i matrix B_2 , and $n_b + n_i = n_t$. For the case where an endpoint is not a collocation point, the grid point nearest to the boundary, at which an explicit boundary condition is given, is considered as a boundary point. All the points near where behavioral boundary conditions are given are not included in this definition. These points are the ones that give rise to the first n_b rows in Eqs. (102) and (103). Note, that this ordering was chosen for clarity in this section.

There is also the Hamiltonian matrix equation

$$n_b \{ \underbrace{\begin{pmatrix} H_{11} - E & H_{12} \\ H_{21} & H_{22} - E \end{pmatrix}}_{n_b + n_i} \begin{pmatrix} \psi_1 \\ \psi_2 \end{pmatrix} \}_{n_i} = 0, \quad (103)$$

where the Hamiltonian matrix has also been divided into four matrices: H_{11} , H_{12} , H_{21} , and H_{22} .

So there are $n_t + n_b$ equations and n_t unknowns (ψ_1 and ψ_2) as well as the eigenvalue. One could approximately solve these equations with singular value decomposition [56], but it is much faster to simply discard the first n_b rows of the Hamiltonian matrix and incorporate the boundary conditions into the remaining eigenvalue problem:

$$(H_{22} - H_{21} B_1^{-1} B_2 - E) \psi_2 = 0, \quad (104)$$

where B_1 has an inverse because all of its rows are linearly independent (otherwise more than one boundary condition would have been specified for a given boundary point). Calculating the inverse is not too computationally expensive because $n_b \ll n_t$. Then solve for ψ_1 afterwards with

$$\psi_1 = -B_1^{-1} B_2 \psi_2. \quad (105)$$

IX. MATRIX METHODS

In one dimension the Hamiltonian matrix for the PS method is dense but in three dimensions with three domains the number of nonzero elements scales as $24n^4$ out of a possible $36n^6$. The boundary condition matrix is also sparse with $8n^4$ nonzero elements out of $48n^5$ (for the simplest case where behavioral conditions are used whenever possible). Therefore, any attempt to solve these equations should take advantage of these memory savings.

Equation (104) is solved by the method of inverse iteration [56] after shifting the eigenvalue with an approximately known value. In cases where the exact eigenvalue is not known *a priori*, one solves the full eigenvalue problem for a low resolution case first and then at each successive iteration shifts the eigenvalue using the result of the previous iteration. Because the Hamiltonian matrix is not symmetric, a complex eigenvalue may occur. There is no theoretical reason prohibiting the numerical eigenvalue from containing an imaginary part at finite resolution but, in fact, none were generated for $n > 5$. Of course, the imaginary part contributes to the error which must converge to zero.

The above solution method can yield highly oscillatory wave functions which appear to diverge on the boundaries of the computational domain. These nonphysical wave functions do not satisfy the first n_b rows of Eq. (103) and arise as an artifact of solving a subset of equations of the overdetermined system. They are easily identified and rejected and in no way affect the true solution.

The entire calculation for $n = 14$ took only about 20 min on a 6-GHz machine. Memory needed to solve the linear equations was the limiting factor because inverting the equation has requirements scaling as n^6 . The generalized *minimal residual* (GMRES) algorithm [89] might reduce the memory requirements of the solution of the linear equations that arise in the inverse iteration. For simplicity of coding, the above calculations were done using MATHEMATICA [90]. Care was taken to use predefined functions whenever such choice was more efficient.

X. RESULTS

This article is an exploration of the PS method as applied to heliumlike systems, not an attempt to improve the energy eigenvalues for bound states. That has already been done to a higher precision than will ever be needed [9–19]. The focus here is on showing that the PS method works in a new application and assessing its convergence properties. Table I gives a list of runs used in this section to discuss the effects of the Coulomb terms, energy level (ground or excited), computational domains and numerical methodology on the convergence of the solution to the two-electron problem.

TABLE I. A list of the different cases that are compared in this section. Exc refers to the first excited S state. Grd refers to the ground state. N_D is the number of domains. B, R, and E refer to behavioral, regularity, and excision, respectively.

Case	Potential		State	Domain	Boundary conditions		
	Z	α	Exc/Grd	N_D	$\rho = 0$	$\phi, \zeta = 0$	$\rho = \infty$
A	1	1	Grd	3	B	B	B
B	1	0	Grd	3	B	B	B
C	2	1	Grd	3	B	B	B
D	2	1	Exc	3	B	B	B
E	1	1	Grd	1	B	B	B
F	1	0	Grd	1	B	B	B
G	1	1	Grd	3	R	B	R
H	1	1	Grd	3	R	B	E
I	1	1	Grd	3	B	R	B
J	1	1	Grd	3	B	E	B

A. Convergence in energy

In this section, the energy error means the difference between the numerical energy eigenvalue at finite resolution and the exact energy eigenvalue of the nonrelativistic infinite-mass-nucleus Hamiltonian. When no analytic value exists, highly precise variationally calculated values are used [9–19].

The energy errors for H^- , H^- with the electron-electron interaction turned off, the ground states of helium, and the first excited S state of helium (cases A, B, C, and D) are shown in Fig. 8. The first important result is that the energies appear to converge in an approximate exponential fashion. Since these are not variational calculations there is no reason to expect monotonically decreasing energy errors. Detailed inspection of the solutions suggests that the kinks in the graphs are discreteness effects. That is, the precise positioning of the grid points has a large effect on the magnitude of the error.

A potentially significant issue is the impact on convergence of logarithmic terms present in the Fock expansion. Prior

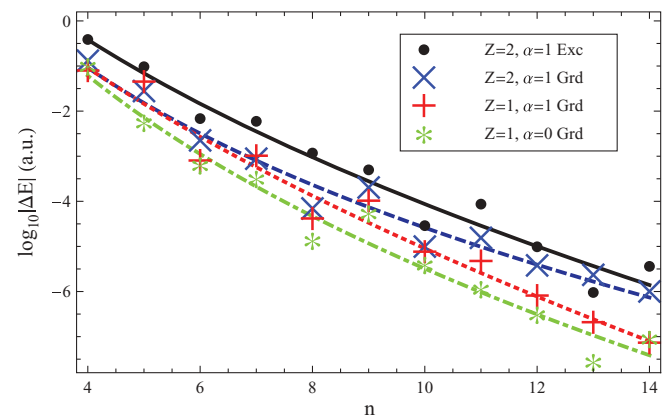


FIG. 8. (Color online) The convergence of the energy of H^- , case A (red pluses), two non-interacting electrons in the field of a proton; case B (green stars), the ground state of He; case C (blue crosses), and its first excited S state; case D (black circles) as a function of grid resolution n , with dotted red, dot-dashed green, dashed blue, and solid black fits, respectively. See Appendix B for fitting functions and method.

authors have been able to calculate very accurate energies without adverse effects of the infinite second derivative at $\rho = 0$, but the PS method is sensitive to singularities anywhere within the domain. Figure 8 includes a calculation of the H^- system with the electron-electron interaction turned off, altering the exact solution and removing the logarithmic term. The rate of convergence is comparable in all cases, suggesting that the influence of the logarithmic term on convergence is subdominant for $n \leq 14$. This conclusion agrees with the analysis in Sec. VIB.

Ideally, the numerical method should handle states other than the ground state. Figure 8 shows the convergence of energies for the ground state and the first excited S state of helium. The important result is that the convergence of both calculations is approximately exponential with a similar rate.

The relative sizes of the magnitude of the error at fixed grid size for H^- , He, and excited He are roughly consistent with the general expectation set by the difficulty in resolving the solution's small-scale structure. Errors for ground state He are larger than H^- because the exponential length scale for falloff of the He wave function is smaller than that of H^- ; errors for the excited state of He are larger than the ground state of He because the oscillatory length scale of the excited state is smaller than the exponential length scale of the ground state.

Figure 9 shows the impact on convergence of using a single numerical subdomain, D_0 , versus three, $\{D_1, D_2, D_3\}$. The single domain had one third as many points as the computation with three domains. However, the resolution in the x direction dominates the convergence and in that dimension the resolution is identical. Domain D_0 has radial-like coordinates near the electron-proton cusp but not near the electron-electron cusp. One anticipates slower convergence in the energy using D_0 . Comparison shows that two interacting electrons on three domains (case A) or two noninteracting electrons on D_0 (case F) have similar exponential rates of convergence. On the other hand, two interacting electrons on D_0 (case E) converge more slowly. This result shows multiple grids are essential for achieving superior convergence and that

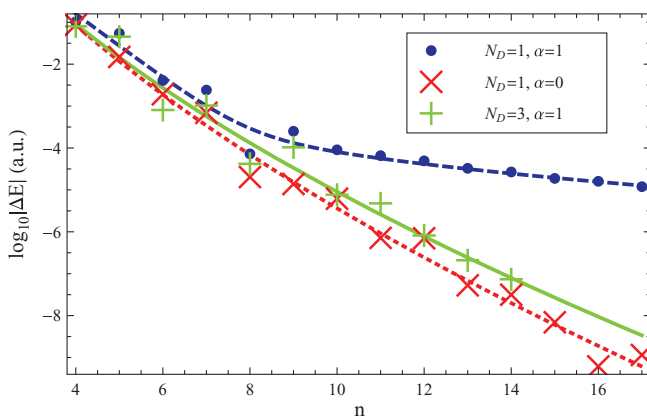


FIG. 9. (Color online) The convergence of the energy of, case E, H^- using only one computational domain with the electron-electron interaction on (blue circles); case F, one domain with the interaction off (red crosses); and case A, three domains with the interaction on (green pluses) with dashed blue, dotted red, and solid green fits, respectively. See Appendix B for fitting functions and method.

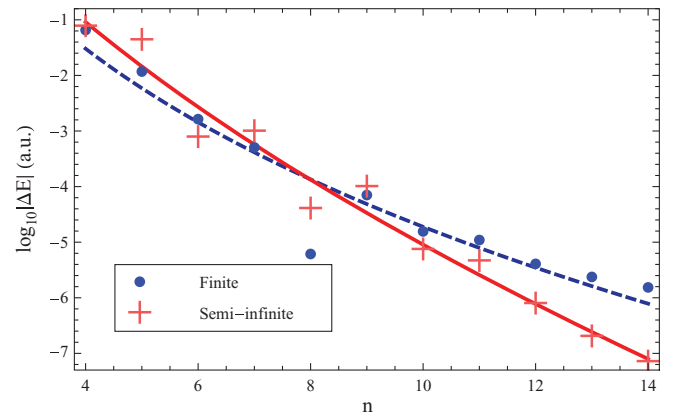


FIG. 10. (Color online) The convergence of the energy of, case H, H^- doing the calculation on a finite domain (blue circles); and case A, semi-infinite domain (red pluses) with dashed blue and solid red fits, respectively. See Appendix B for fitting functions and method.

the electron-electron cusp drives this requirement. If the single domain data were adjusted to account for the fact that they used fewer points, they would be shifted to the left by a factor of $3^{1/3} \approx 1.44$. This would not affect the conclusion that using three domains is more efficient because the single domain solution is only algebraically convergent starting at about $n = 8$. Using three subdomains is more efficient because the work involved in the calculation has the same scaling whether one or three subdomains is used.

Figure 10 presents a comparison of calculations having the full semi-infinite domain (case A) to those with a finite cutoff in ρ (case H). The scaling of the cutoff $\rho_{\max} \propto \sqrt{n}$ imposed in case H is derived in Appendix A by balancing the error due to finite resolution from the numerical scheme with errors introduced by truncating the bound state. The figure shows that the semi-infinite calculation fares better. This is a consequence of the two different sets of assumptions used to distribute the points. The grid points in the semi-infinite scheme are more often found where the wave function is large. Half the points have $\rho < 1$ ($x > 0$) because 0 is the center of the x dimension. By comparison, half the points have $\rho < \rho_{\max}/2$ in the finite calculation. The number of points where the wave function is large is smaller in this latter scheme. Although the semi-infinite strategy is more effective, nothing can be said about the optimal strategy because other distribution methods were not considered. The main advantage of the method is simplicity since there are no adjustable parameters.

Figure 11 presents a comparison of the different ways of handling the regularity of the wave function at the two-particle coalescence points. The simplest method, relying on the regularity of the Chebyshev polynomials (case A), does as well or better than the other methods (cases I and J).

Figure 12 compares two ways of handling the wave function at $\rho = 0$, case A, relying on the regularity of the Chebyshev polynomials (behavioral) and case G, directly specifying a logarithmic derivative (regularity). The latter method is slightly better but both have roughly the same convergence rate.

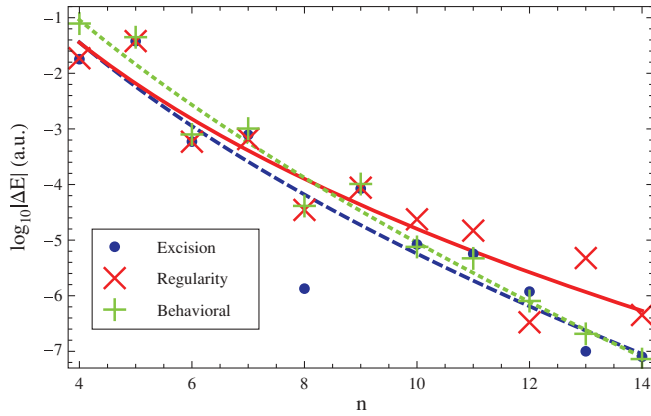


FIG. 11. (Color online) The convergence of the energy of H^- using three different methods of ensuring regularity at the two-particle coalescence points: case A, relying on the regularity of the Chebyshev polynomials (green pluses); case I, using the Kato cusp condition as a regularity condition (red crosses); and case J, excising the singularity (blue circles) with green dotted, solid red, and dashed blue fits, respectively. See Appendix B for fitting functions.

B. Convergence in local energy

Another useful measure of convergence is the local energy,

$$E_{\text{loc}} = \frac{\mathcal{H}\psi}{\psi}. \quad (106)$$

which is constant only for an exact eigenfunction ψ of Hamiltonian \mathcal{H} . Throughout this subsection all analysis and data refers to case A.

The difference between the local energy and the numerically evaluated eigenvalue E gives a local measure of the error in ψ in a particular calculation. Define

$$\Delta E_{\text{loc}} = E_{\text{loc}} - E. \quad (107)$$

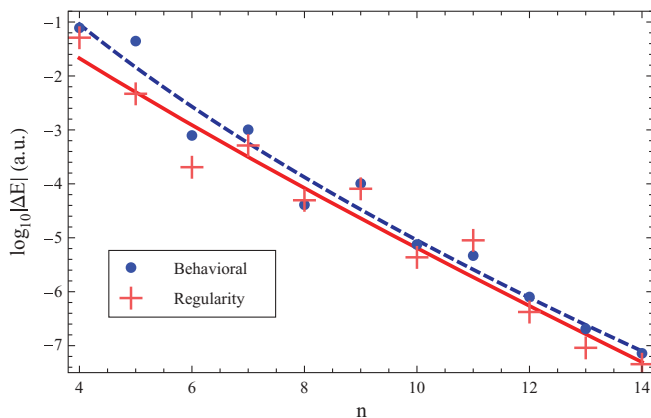


FIG. 12. (Color online) The convergence of the energy of H^- using two different methods of ensuring regularity at the three-particle coalescence point: case A, relying on the regularity of the Chebyshev polynomials (blue circles); and case G, using the Fock condition to specify a logarithmic derivative (red pluses) with dashed blue and solid red fits, respectively. See Appendix B for fitting functions and method.

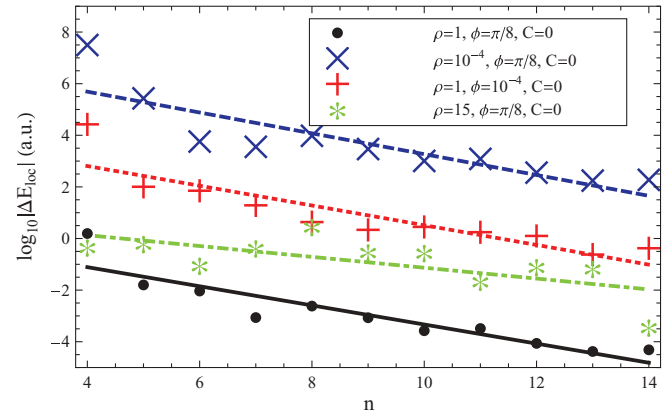


FIG. 13. (Color online) The convergence of the local energy of H^- at four points in the domain: the center of the computational domain (black circles), near the triple coalescence point (blue crosses), near the proton-electron coalescence point (red pluses), and at large ρ (green stars). Their geometric fits are given by the solid black, dashed blue, dotted red, and dot-dashed green lines, respectively. See Appendix B for fitting functions and method.

For the PS method, ΔE_{loc} is zero at all grid points (subject to limits of finite precision arithmetic). Nonzero differences exist between grid points. Figure 13 illustrates the convergence of local energy at four different points. Of the four points, the error in local energy is lowest at the point in the center of the computational domain ($\{\rho, \phi, C\} = \{1, \pi/8, 0\}$). It is larger in magnitude near the singularities ($\{\rho, \phi, C\} = \{10^{-4}, \pi/8, 0\}$ and $\{1, 10^{-4}, 0\}$) because near these points $E_{\text{loc}} \rightarrow \infty$ for any nonexact ψ . However, the geometric fits show that the rate of convergence is approximately the same at all three of those points. A different behavior is seen at $\{\rho, \phi, C\} = \{15, \pi/8, 0\}$. The error is roughly constant over much of the graph but begins to decrease at high resolution. This is not surprising given the fact that there are only a few grid points at such large hyperradius.

Figure 14 displays the convergence of the local energy as a function of x at fixed angular coordinates. For a perfect exponential decrease in local energy error, the curves would be equidistant from each other. This is approximately true throughout the domain except near $x = \pm 1$ (small and large ρ).

If the numerical solution is considered to be trustworthy where the local energy error is less than some threshold (e.g., $|\Delta E_{\text{loc}}| < 10^{-2}$), then the wave function is well represented in an intermediate range of ρ ($10^{-2} < \rho < 10^{1.3}$) but not near the triple coalescence point nor at infinity.¹⁰

At large ρ ($x \approx -1$), the true wave function falls off exponentially (in fact, with respect to the x coordinate it falls off even faster). The PS method represents the exponential in terms of a polynomial. When one extrapolates using the polynomial to $x = -1$, the wave function is small but nonzero

¹⁰The error in the function value is roughly constant everywhere in the domain, but the magnitude of derivatives and the wave function becomes large compared to the magnitude of the wave function at small and large ρ .

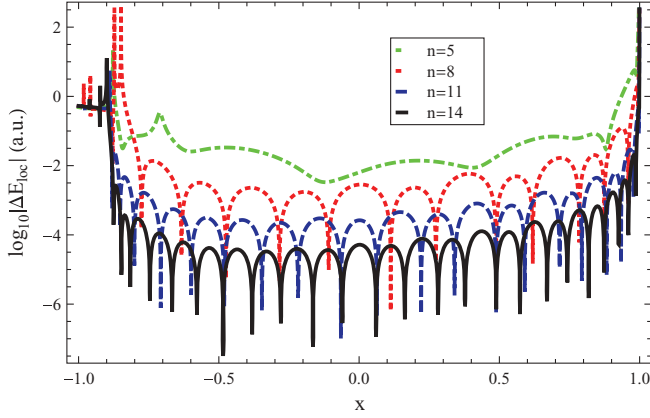


FIG. 14. (Color online) The error in the local energy of H^- as a function of x with $r_1 = 2r_2$, and $C = -1$ (the electrons are on the same side of the nucleus) at four different resolutions: $n = 5$ green dot-dashed, $n = 8$ red dotted, $n = 11$ blue dashed, $n = 14$ black solid.

(the exact value should be zero). However, the Hamiltonian acting on the polynomial is guaranteed to be zero because every coefficient in the Hamiltonian operator has a factor of $(1+x)$. So

$$\lim_{\rho \rightarrow \infty} \frac{\mathcal{H}\psi}{\psi} = 0, \quad (108)$$

and $\Delta E_{\text{loc}} \rightarrow -E$, a constant at large ρ as seen in Fig. 14. Detailed inspection of the data near $x = -1$ suggests that for any finite ρ there exists a resolution above which the solution becomes trustworthy.

The local energy behavior near the triple-coalescence point ($\rho = 0$) is of special interest as a probe of the wave function's nonanalytic behavior. Figure 15 displays ΔE_{loc} as a function of θ_{12} , the angle between the two electrons, for fixed r_2/r_1 and for a number of choices of ρ , following a similar figure from Myers *et al.* [78]. In this small ρ regime, the terms that dominate the Hamiltonian are the kinetic energies in the various directions. Each of these, individually, scales as $1/\rho^2$

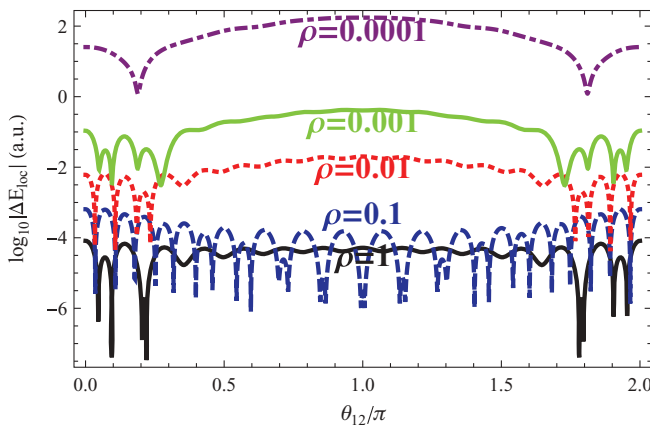


FIG. 15. (Color online) The error in local energy of H^- plotted at different values of the angle θ_{12} with $r_1 = 2r_2$ and at resolution $n = 14$ and at $\rho = 1$ (solid black), $\rho = 0.1$ (dashed blue), $\rho = 0.01$ (dotted red), $\rho = 0.001$ (solid green), and $\rho = 0.0001$ (dot-dashed purple).

[see Eq. (25)]. For the exact solution, these terms cancel each other, but for almost any solution which is not exact, the local energy scales as $1/\rho^2$. This scaling is shown in Figs. 14 and 15. Again detailed inspection of the data near $x = 1$ suggests that for any finite nonzero ρ there exists a resolution above which the solution becomes trustworthy. Furthermore, Fig. 13 shows that there is no sign of the convergence rate being slowed due to the logarithmic terms at this resolution.

C. Cauchy errors

Throughout this subsection all data refers to cases A, B, and C. The Cauchy error is a measure of the difference between numerical solutions with different resolution. One such measure is the normed quantity

$$\Delta_n = \sqrt{\int d^3r_1 d^3r_2 (\psi_n - \psi_{n-1})^2}. \quad (109)$$

The true ψ satisfies

$$1 = \int d^3r_1 d^3r_2 \psi^2, \quad (110)$$

but integrating ψ_n all the way to $\rho = \infty$ would diverge. This is a consequence of having small but nonzero errors at $\rho = \infty$ in the value of ψ_n . An upper limit $\rho = 10$ is adopted in the normalization of ψ_n and calculation of Δ_n . It is arbitrary but encompasses most of the physical extent of the solution. The Cauchy error in any subinterval of the full interval must converge. To the extent that the error in the interval calculated is dominant, the rate of convergence can be assessed.

Figure 16 gives Δ_n as a function of resolution while Fig. 17 gives the pointwise difference at $\rho = 0$ where the wave function is maximum. Both plots show that convergence is approximately exponential.

D. The logarithmic derivative at the triple coalescence point

Throughout this subsection all data refers to cases A, B, and C. The only direct evidence that the convergence of the

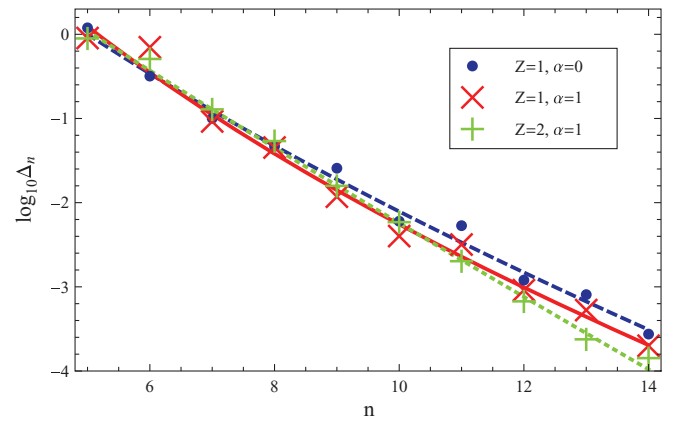


FIG. 16. (Color online) The root-mean-square average Cauchy error is plotted with increasing resolution for three cases: H^- with noninteracting electrons (blue circles); H^- with interacting electrons (red crosses); and helium with interacting electrons (green pluses) with dashed blue, solid red, and dotted green fits, respectively. See Appendix B for fitting functions and method.

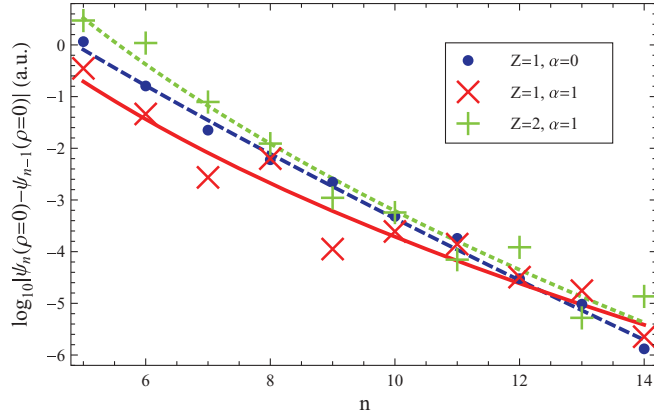


FIG. 17. (Color online) Pointwise differences in the wave function evaluated at $\rho = 0$ for increasing resolution for three cases: H^- with noninteracting electrons (blue circles); H^- with interacting electrons (red crosses); and helium with interacting electrons (green pluses) with dashed blue, solid red, and dotted green fits, respectively. See Appendix B for fitting functions and method.

solutions is slowed by the logarithmic terms in the exact solution comes from evaluating the logarithmic derivative with respect to ρ at $\rho = 0$. The exact value is

$$\left. \frac{\partial_x \psi}{\psi} \right|_{x=1} = -\frac{1}{2} \left\{ -Z(\cos \phi + \sin \phi) + \frac{\alpha}{2} \sigma[C, \phi] \right\}. \quad (111)$$

The root-mean-square error is

$$\delta_{\text{RMS}} = \sqrt{\int \int d\Omega \left(\frac{\partial_x \psi}{\psi} - \frac{\partial_x \psi_n}{\psi_n} \right)_{x=1}^2}, \quad (112)$$

where

$$\int \int d\Omega = \int_0^{\pi/4} d\phi \sin^2 2\phi \int_{-1}^1 dC. \quad (113)$$

Figure 18 displays δ_{RMS} . Turning off the electron-electron interaction, the convergence is noticeably faster. The important

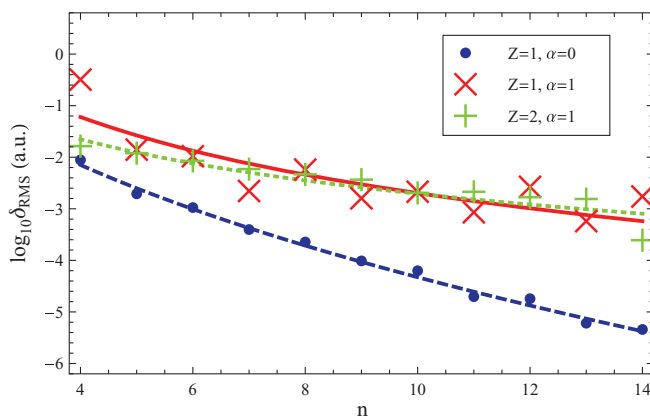


FIG. 18. (Color online) The root mean square error in the logarithmic derivative evaluated at $\rho = 0$ with increasing resolution for three cases: H^- with noninteracting electrons (blue circles); H^- with interacting electrons (red crosses); and helium with interacting electrons (green pluses) with dashed blue, solid red, and dotted green fits, respectively. See Appendix B for fitting functions and method.

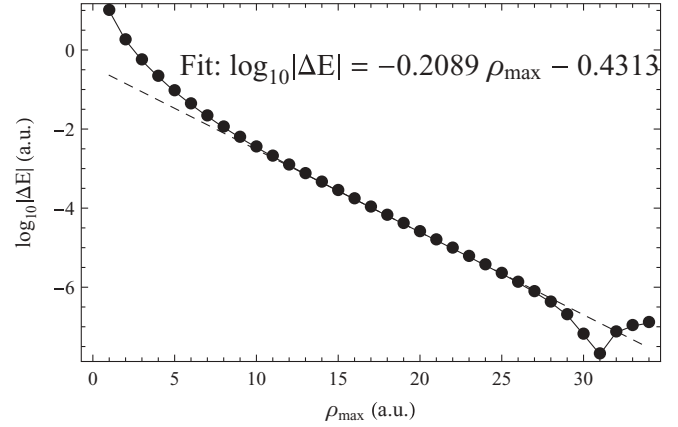


FIG. 19. Energy error from truncation as a function of ρ_{max} with a fit to the points from $\rho_{\text{max}} = 15$ to $\rho_{\text{max}} = 25$.

conclusion is that the wave functions' convergence is indistinguishable from exponentially fast, while the convergence of its derivatives, at least near $\rho = 0$ is slower. Of course, the second derivative with respect to ρ is infinitely wrong at $\rho = 0$. It converges to a finite value, and the exact value is infinite.

XI. CONCLUSION

This article demonstrates the application of PS methods for solving the nonrelativistic Schrödinger equation for a system with two electrons. The method successfully handled both ground and excited S states of heliumlike systems. The rate of convergence for most properties measured was indistinguishable from being exponentially fast. Local errors decrease in the same manner.

The choice of variables in the vicinity of the two-particle coalescence and the use of multiple, overlapping domains are the critical requirements. These are important so the PS method can represent the analytic form of the solution near all the two-particle cusps and ensure a more efficient algorithm. In other respects the most straightforward choices work well. For example, grid points are determined by the roots of Chebyshev

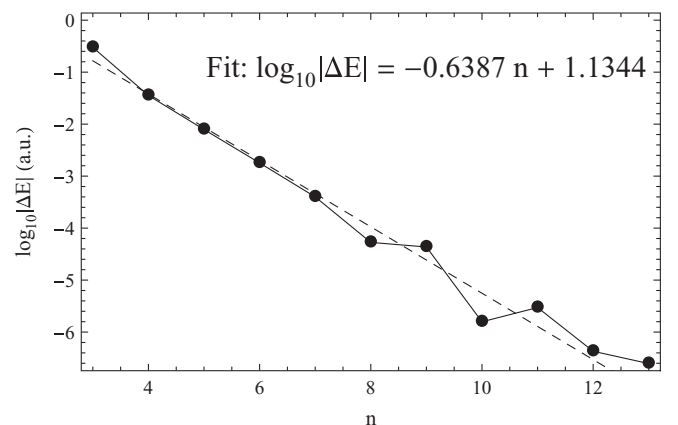


FIG. 20. Energy error from finite resolution as a function of resolution at $\rho_{\text{max}} = 20$ with a fit.

TABLE II. The algebraic fits of quantities, Q , displayed in figures throughout the article.

Q	Figure number	a_1	Δa_1	a_2	Δa_2
$\delta_{\text{RMS}}^N[g_1]$	1	0.470	0.189	-1.852	0.206
$\delta_{\text{RMS}}(Z = 1, \alpha = 1)$	18	10.3	6.1	-3.71	0.27
$\delta_{\text{RMS}}(Z = 2, \alpha = 1)$	18	0.883	0.275	-2.65	0.14

polynomials, which experience shows generally produce the best convergence in PS methods [3,55]. Behavioral boundary conditions (no explicit regularity conditions) are sufficient to handle the wave function in the vicinity of the coalescence points and also produce convergence as good as or better than the other possibilities tested.

The energy eigenvalue found by the variational method converges most efficiently when basis functions which behave like the exact solution are included but this selection process can be time-consuming and problematic. Of course, much higher precision than reported here was obtained long ago by variational methods. The PS method has the advantage in new and possibly also in more complex applications of not needing the same sort of specialized tuning that has benefited variational calculations. Although this article does not attempt to reproduce the ultra-high-precision results achieved by variational methods it strongly suggests that the PS method will ultimately prove to be a superior approach for reaching such results in systems with a small number of electrons.

The local energy is not directly controlled when total energy is minimized. Local energy minimization schemes exist and

TABLE III. The geometric fits of quantities, Q , displayed in figures throughout the article.

Q	Figure number	a_1	Δa_1	a_2	Δa_2
$ \Delta E_{\text{loc}} ^a$	13	2.35	1.97	0.426	0.037
$ \Delta E_{\text{loc}} ^b$	13	2.02×10^7	2.42×10^7	0.395	0.050
$ \Delta E_{\text{loc}} ^c$	13	21700	21900	0.415	0.044
$ \Delta E_{\text{loc}} ^d$	13	9.33	10.73	0.616	0.074

^a $\rho = 1, \phi = \pi/8, C = 0.$

^b $\rho = 10^{-4}, \phi = \pi/8, C = 0.$

^c $\rho = 1, \phi = 10^{-4}, C = 0.$

^d $\rho = 15, \phi = \pi/8, C = 0.$

have the advantage that excited states are found at local minima of the variance in local energy instead of just the ground state as is true for the standard variational method [31]. However, they lead to nonlinear problems which may be difficult to handle numerically (minimization of the variance in local energy with respect to parameters in the trial wave function), but still tractable because one need not calculate the energy at each step. By contrast, the PS method controls local energy while the numerical solution remains a linear one. At the same time, the PS method is superior in terms of its convergence rate to other direct partial differential equation solvers (grid based methods) such as finite differencing and finite element which also control the local error.

We plan to extend the method to calculate non- S states and continuum two-electron states to compute the photoabsorption bound-free cross sections with both initial and final states evaluated with the same methodology.

TABLE IV. The supergeometric or subgeometric fits of quantities, Q , displayed in figures throughout the article.

Q	Fig(s).	a_1	Δa_1	a_2	Δa_2	a_3	Δa_3
$\delta_{\text{RMS}}^N[g_2]$	1	0.895	0.070	0.4031	0.0015	1.3846	0.0017
$ \Delta H_N^{\text{max}} (\alpha = 1)$	3	936	418	0.5943	0.0089	0.8348	0.0067
$ \Delta H_N^{\text{max}} (\alpha = 0)$	3	14.6	6	0.3282	0.0073	0.7209	0.0047
$ (\Delta H_N)^{\text{rs}} (\alpha = 0)$	4	181	84	2.90×10^{-6}	3.1×10^{-7}	0.3733	0.0020
$ \Delta E $ (Case A)	8,9,10,11,12	121000	64000	0.00138	0.00022	0.549	0.01
$ \Delta E $ (Case B)	8	1.17×10^{11}	6.7×10^{10}	1.53×10^{-8}	4.3×10^{-9}	0.3262	0.0070
$ \Delta E $ (Case C)	8	1.28×10^{11}	5.7×10^{10}	5.71×10^{-9}	1.39×10^{-9}	0.2796	0.0057
$ \Delta E $ (Case D)	8	1.62×10^6	880000	0.000385	0.000073	0.478	0.011
$ \Delta E $ (Case F)	9	286000	126000	0.00100	0.00012	0.5604	0.0069
$ \Delta E $ (Case G)	12	30	19.3	0.0972	0.0100	0.819	0.019
$ \Delta E $ (Case H)	10	2.10×10^{10}	1.52×10^{10}	5.73×10^{-9}	2.36×10^{-9}	0.2614	0.0097
$ \Delta E $ (Case I)	11	3.89×10^9	3.10×10^9	4.08×10^{-8}	1.73×10^{-8}	0.289	0.011
$ \Delta E $ (Case J)	11	5.26×10^6	5.68×10^6	0.0000263	0.0000114	0.417	0.018
$\Delta_n(Z = 1, \alpha = 0)$	16	7260	1200	0.0394	0.0016	0.6282	0.0053
$\Delta_n(Z = 1, \alpha = 1)$	16	2.77×10^6	590000	0.000876	0.000068	0.4541	0.0047
$\Delta_n(Z = 2, \alpha = 1)$	16	472	58	0.2406	0.0038	0.9001	0.0047
$ \psi_n - \psi_{n-1} ^a$	17	27300	5900	0.0520	0.0019	0.7833	0.0052
$ \psi_n - \psi_{n-1} ^b$	17	1.17×10^{12}	6.9×10^{11}	1.49×10^{-8}	4.5×10^{-9}	0.3046	0.0073
$ \psi_n - \psi_{n-1} ^c$	17	1.63×10^{14}	8.6×10^{13}	1.49×10^{-8}	3.6×10^{-9}	0.3475	0.0059
$\delta_{\text{RMS}}(Z = 1, \alpha = 0)$	18	170	23	0.00418	0.00022	0.4404	0.0041

^a $\rho = 0, Z = 1, \alpha = 0.$

^b $\rho = 0, Z = 1, \alpha = 1.$

^c $\rho = 0, Z = 2, \alpha = 1.$

TABLE V. The mixed geometric and algebraic fits of quantities, Q , displayed in figures throughout the article.

Q	Fig.	a_1	Δa_1	a_2	Δa_2	a_3	Δa_3	a_4	Δa_4
$ \Delta f[\rho = 10^{-6}] $	2	0.0818	0.0487	0.696	0.022	0.295	0.113	-3.822	0.092
$ \Delta f[\rho = 10^{-1}] $	2	0.0264	0.0306	0.725	0.027	0.472	0.595	-5.172	0.290
$ \Delta f[\rho = 10^4] $	2	0.161	0.112	0.743	0.011	1.29×10^{-7}	2.16×10^{-7}	-2.460	0.372
$ (\Delta H_N)^{i*} ^a$	4	1.96×10^{-7}	1.36×10^{-7}	0.491	0.018	0.263	0.091	-10.358	0.083
$ \Delta E $ (Case E)	9	193	140	0.169	0.021	0.190	0.087	-3.39	0.18

^a $\alpha = 1$.

ACKNOWLEDGMENTS

We thank Saul Teukolsky, Harald Pfeiffer, Cyrus Umrigar, Ira Wasserman, Sharvari Nadkarni-Ghosh, and Sergei Dyda for helpful conversations. This material is based on work supported by the National Science Foundation under Grant No. AST-0406635.

APPENDIX A: SETTING ρ_{\max} FOR THE TRUNCATED DOMAIN

When truncating the domain at a finite ρ , it is wise to balance the error produced by the cutoff with that given by the finite resolution. The former was studied by calculating the energy of case H as a function of ρ_{\max} . Figure 19 shows that difference between the truncated energy and the correct value of the H^- energy falls off as an exponential. The calculation was done with $n = 14$. We see at large values of ρ_{\max} that this finite resolution ruins the exponential behavior. There is a minimum at $\rho_{\max} = 31$. This is probably where the resolution error happens to cancel the truncation error. At larger ρ_{\max} , the resolution error dominates. Therefore, only the points with $15 \leq \rho_{\max} \leq 25$ were used for the fit, $\log_{10} |\Delta E| = A\rho_{\max} + B$. A and B were found to be -0.2089 and -0.4313 , respectively.

In order to measure the effect of finite resolution ρ_{\max} was fixed at 20 and the difference between the energy at resolution n and 14 was plotted in Fig. 20. The error from resolution effects should increase when ρ_{\max} is increased because the density of points goes down. So the resolution error is assumed to be of the form $\log_{10} |\Delta E| = Cn/\rho_{\max} + D$. $C/20$ and D were found to be -0.6387 and 1.1344 , respectively.

Setting the two errors equal to each other yields the formula

$$\rho_{\max} = -3.7476 + 7.8100\sqrt{n + 0.2297}. \quad (\text{A1})$$

It is technically possible to get better energies as was shown in Fig. 19 (due to error cancellations), but taking advantage of that kind of effect is fine-tuning.

APPENDIX B: FITS

Numerical rates for convergence are summarized in Tables II, III, IV, and V. The method is as follows: let Q_n be the quantity converging to zero as n goes to infinity, consider fitting functions of the forms

$$f_{\text{geom}}[n] = a_1(a_2)^n \quad (\text{B1})$$

$$f_{\text{alg}}[n] = a_1 n^{a_2} \quad (\text{B2})$$

$$f_{\text{sup/sub}}[n] = a_1(a_2)^{n^{a_3}} \quad (\text{B3})$$

$$f_{\text{geom/alg}}[n] = a_1(a_2)^n + a_3 n^{a_4}, \quad (\text{B4})$$

which are geometric, algebraic, supergeometric ($a_3 > 1$), or subgeometric ($a_3 < 1$) and mixed geometric and algebraic fits, respectively. A χ^2 fitting method is used:

$$\chi^2 = \sum_n \left(\log_{10} \left| \frac{Q_n}{f[n]} \right| \right)^2, \quad (\text{B5})$$

where Q_n is the quantity Q evaluated at resolution n and the sum over n goes from the even numbers from 8 to 100 for the one-dimensional models, 5 to 14 for the Cauchy errors, and from 4 to 14 for all others. χ^2 is minimized with respect to all a_i for the fit which is most reasonable on theoretical grounds. Errors in the a_i are estimated by calculating

$$\Delta a_i = \sqrt{\frac{\chi^2}{\partial_{a_i} \chi^2}} \quad (\text{B6})$$

at the minimum of χ^2 . Of course large error in the values of amplitudes a_1 and a_3 for the mixed geometric and algebraic fit imply that the other parameters that multiply that amplitude may be meaningless.

- [1] R. Wildt, *Astrophys. J.* **190**, 611 (1939).
[2] T. L. John, *Astron. Astrophys.* **193**, 189 (1988).
[3] J. P. Boyd, *Chebyshev and Fourier Spectral Methods*, 2nd edition (Dover, Mineola, NY, 2000).
[4] V. E. A. Hylleraas, *Z. Phys.* **54**, 347 (1929).
[5] C. L. Pekeris, *Phys. Rev.* **112**, 1649 (1958).
[6] C. L. Pekeris, *Phys. Rev.* **126**, 1470 (1962).
[7] K. Frankowski and C. L. Pekeris, *Phys. Rev.* **146**, 46 (1966).
[8] Y. Accad, C. L. Pekeris, and B. Schiff, *Phys. Rev. A* **4**, 516 (1971).
[9] J. D. Baker, D. E. Freund, R. N. Hill, and J. D. Morgan, *Phys. Rev. A* **41**, 1247 (1990).
[10] G. W. F. Drake, *Phys. Scr.* **T 83**, 83 (1999).
[11] V. I. Korobov, *Phys. Rev. A* **61**, 064503 (2000).
[12] A. M. Frolov, *Phys. Rev. E* **62**, 8740 (2000).
[13] V. I. Korobov, *Phys. Rev. A* **66**, 024501 (2002).
[14] G. W. F. Drake, M. M. Cassar, and R. A. Nistor, *Phys. Rev. A* **65**, 054501 (2002).
[15] A. M. Frolov, *Phys. Rev. E* **74**, 027702 (2006).
[16] A. M. Frolov, *J. Phys. A* **40**, 6175 (2007).

- [17] H. Nakashima and H. Nakatsuji, *J. Chem. Phys.* **127**, 224104 (2007).
- [18] H. Nakashima and H. Nakatsuji, *J. Chem. Phys.* **128**, 154107 (2008).
- [19] Y. I. Kurokawa, H. Nakashima, and H. Nakatsuji, *Phys. Chem. Chem. Phys.* **10**, 4486 (2008).
- [20] T. Kinoshita, *Phys. Rev.* **105**, 1490 (1957).
- [21] H. M. Schwartz, *Phys. Rev.* **120**, 483 (1960).
- [22] C. Schwartz, *Phys. Rev.* **128**, 1146 (1962).
- [23] A. J. Thakkar and T. Koga, *Theor. Chim. Acta* **109**, 36 (2003).
- [24] R. C. Forrey, *Phys. Rev. A* **69**, 022504 (2004).
- [25] J. H. Bartlett, J. J. Gibbons, and C. G. Dunn, *Phys. Rev.* **47**, 679 (1935).
- [26] J. H. Bartlett, *Phys. Rev.* **51**, 661 (1937).
- [27] B. Klahn and J. D. Morgan III, *J. Chem. Phys.* **81**, 410 (1984).
- [28] C. Schwartz, *Int. J. Mod. Phys. E* **15**, 877 (2006).
- [29] J. H. Bartlett, *Phys. Rev.* **98**, 1067 (1955).
- [30] R. L. Coldwell, *Int. J. Quantum Chem.* **12**, 215 (1977).
- [31] C. J. Umrigar, K. G. Wilson, and J. W. Wilkins, *Phys. Rev. Lett.* **60**, 1719 (1988).
- [32] A. Kono and S. Hattori, *Phys. Rev. A* **29**, 2981 (1984).
- [33] A. Kono and S. Hattori, *Phys. Rev. A* **31**, 1199 (1985).
- [34] M. Griebel and J. Hamaekers, *Mathematical Modelling and Numerical Analysis* **41**, 215 (2007).
- [35] M. I. Haftel and V. B. Mandelzweig, *Ann. Phys. (NY)* **150**, 48 (1983).
- [36] M. I. Haftel and V. B. Mandelzweig, *Phys. Lett. A* **120**, 232 (1987).
- [37] M. I. Haftel and V. B. Mandelzweig, *Phys. Rev. A* **38**, 5995 (1988).
- [38] M. I. Haftel and V. B. Mandelzweig, *Ann. Phys. (NY)* **189**, 29 (1989).
- [39] M. I. Haftel and V. B. Mandelzweig, *Phys. Rev. A* **42**, 6324 (1990).
- [40] R. Krivec, M. I. Haftel, and V. B. Mandelzweig, *Phys. Rev. A* **44**, 7158 (1991).
- [41] R. Krivec, V. B. Mandelzweig, and K. Varga, *Phys. Rev. A* **61**, 062503 (2000).
- [42] P. G. Burke and K. A. Berrington, *Atomic and Molecular Processes: An R-Matrix Approach* (IOP, Bristol, 1993).
- [43] W. M. Huo, in *Computational Methods for Electron-Molecule Collisions*, edited by W. M. Huo and F. Gianturco (Plenum, New York, 1995), chap. 15.
- [44] T. N. Rescigno, C. W. McCurdy, A. E. Orel, and B. H. Lengsfeld, III, in *Computational Methods for Electron-Molecule Collisions*, edited by W. M. Huo and F. Gianturco (Plenum, New York, 1995), chap. 1.
- [45] N. W. Winter, D. Diestler, and V. McKoy, *J. Chem. Phys.* **48**, 1879 (1968).
- [46] C. G. Barraclough and J. R. Mooney, *J. Chem. Phys.* **54**, 35 (1971).
- [47] I. L. Hawk and D. L. Hardcastle, *Comput. Phys. Commun.* **16**, 159 (1979).
- [48] S. Edvardsson, D. Berg, and P. Uddholm, *Comput. Phys. Commun.* **165**, 260 (2005).
- [49] F. S. Levin and J. Shertzer, *Phys. Rev. A* **32**, 3285 (1985).
- [50] M. Braun, W. Schweizer, and H. Herold, *Phys. Rev. A* **48**, 1916 (1993).
- [51] J. Ackermann and J. Shertzer, *Phys. Rev. A* **54**, 365 (1996).
- [52] W. Schweizer, P. Fabinder, R. González-Ferez, M. Braun, S. Kulla, and M. Stehle, *J. Comput. Appl. Math.* **109**, 95 (1999).
- [53] W. Zheng and L.-A. Ying, *Int. J. Quantum Chem.* **97**, 659 (2004).
- [54] W. Zheng and L. an Ying, *SIAM J. Numer. Anal.* **42**, 49 (2004).
- [55] B. Fornberg, *A Practical Guide to Pseudospectral Methods* (Cambridge University Press, New York, 1996).
- [56] W. H. Press, S. A. Teukolsky, W. T. Vetterling, and B. P. Flannery, *Numerical Recipes: The Art of Scientific Computing* (Cambridge University Press, New York, 2007).
- [57] C. Canuto, M. Hussaini, A. Quarteroni, and T. Zang, *Spectral Methods in Fluid Dynamics* (Springer, Berlin, 1988).
- [58] S. Bonazzola, E. Gourgoulhon, and J. A. Marck, *J. Comput. Appl. Math.* **109**, 433 (1999).
- [59] H. P. Pfeiffer, L. E. Kidder, M. A. Scheel, and S. A. Teukolsky, *Comput. Phys. Commun.* **152**, 253 (2003).
- [60] L. E. Kidder and L. S. Finn, *Phys. Rev. D* **62**, 084026 (2000).
- [61] E. Fattal, R. Baer, and R. Kosloff, *Phys. Rev. E* **53**, 1217 (1996).
- [62] A. G. Borisov, *J. Chem. Phys.* **114**, 7770 (2001).
- [63] J. P. Boyd, C. Rangan, and P. H. Bucksbaum, *J. Comput. Phys.* **188**, 56 (2003).
- [64] J. S. Heyl and A. Thirumalai, e-prints arXiv:0903.0020 (2009).
- [65] R. A. Friesner, *Chem. Phys. Lett.* **116**, 39 (1985).
- [66] R. A. Friesner, *J. Chem. Phys.* **85**, 1462 (1986).
- [67] R. A. Friesner, *J. Chem. Phys.* **86**, 3522 (1987).
- [68] M. N. Ringnalda, M. Belhadj, and R. A. Friesner, *J. Chem. Phys.* **93**, 3397 (1990).
- [69] B. H. Greeley, T. V. Russo, D. T. Mainz, R. A. Friesner, J.-M. Langlois, W. A. Goddard III, J. Robert, E. Donnelly, and M. N. Ringnalda, *J. Chem. Phys.* **101**, 4028 (1994).
- [70] R. B. Murphy, M. D. Beachy, R. A. Friesner, and M. N. Ringnalda, *J. Chem. Phys.* **103**, 1481 (1995).
- [71] R. B. Murphy, Y. Cao, M. D. Beachy, M. N. Ringnalda, and R. A. Friesner, *J. Chem. Phys.* **112**, 10131 (2000).
- [72] C. Ko, D. K. Malick, D. A. Braden, R. A. Friesner, and T. J. Martínez, *J. Chem. Phys.* **128**, 104103 (2008).
- [73] G. Arfken, *Mathematical Methods for Physicists* (Academic Press, New York, 1970), chap. 9.
- [74] T. Kato, *Transactions of the American Mathematical Society* **70**, 212 (1951).
- [75] T. Kato, *Transactions of the American Mathematical Society* **70**, 195 (1951).
- [76] A. K. Bhatia and A. Temkin, *Rev. Mod. Phys.* **36**, 1050 (1964).
- [77] A. K. Bhatia and A. Temkin, *Phys. Rev.* **137**, A1335 (1965).
- [78] C. R. Myers, C. J. Umrigar, J. P. Sethna, and J. D. Morgan, *Phys. Rev. A* **44**, 5537 (1991).
- [79] T. Kato, *Commun. Pure Appl. Math.* **10**, 151 (1957).
- [80] R. T. Pack and W. B. Brown, *J. Chem. Phys.* **45**, 556 (1966).
- [81] V. A. Fock, *Izv. Akad. Nauk. SSSR, Ser. Fiz* **18**, 161 (1954).
- [82] V. A. Fock, *D. Kngl. Norske Videnskab. Selsk. Forh.* **31**, 138 (1958).
- [83] P. C. Abbott and E. N. Maslen, *J. Phys. A: Gen. Phys.* **20**, 2043 (1987).
- [84] J. E. Gottschalk, P. C. Abbott, and E. N. Maslen, *J. Phys. A: Gen. Phys.* **20**, 2077 (1987).
- [85] J. E. Gottschalk and E. N. Maslen, *J. Phys. A: Gen. Phys.* **20**, 2781 (1987).

- [86] K. McIsaac and E. N. Maslen, *Int. J. Quantum Chem.* **31**, 361 (1987).
- [87] J. D. Morgan, *Theor. Chim. Acta* **69**, 181 (1986).
- [88] W. B. Brown and R. J. White, *Phys. Rev. Lett.* **18**, 1037 (1967).
- [89] M. Barrett, M. Berry, T. F. Chan, J. V. der Horst, and H. V. der Horst, *Templates for the Solution of Linear Systems: Building Blocks for Iterative Methods* (SIAM, Philadelphia, PA, 1994).
- [90] I. Wolfram Research, *MATHEMATICA*, version 6.0 (Wolfram Research, Inc., Champaign, Illinois, 2007).